UNIVERSITÀ DEGLI STUDI DI UDINE
hic sunt futura
www.uniud.it

UNIVERSITY OF UDINE

Department of Medical Area (DAME)

Phd Course in Biomedical and Biotechnological Sciences

(in agreement with National Cancer Institute, CRO Aviano)

XXIV Cycle

Phd Thesis

ROLE OF THE EXTRACELLULAR MATRIX PROTEIN EMILIN1 IN MAMMARY GLAND DEVELOPMENT AND IN Δ16HER2-DRIVEN TUMORIGENESIS

Phd Student
ANDREA FAVERO

Phd Coordinator
PROF. ALESSANDRA CORAZZA

Supervisors
DR. PAOLA SPESSOTTO
DR. BARBARA BELLETTI

YEAR 2022

Table of contents

ABSTRACT

ABSTRACT

HER2-positive breast cancers (BC) account for 15-20% of invasive BC and are usually characterized by poor prognosis. The expression of the Δ16HER2 splicing variant in a subset of HER2-amplified BC is associated with an increased transforming activity. The extracellular matrix (ECM) plays a fundamental role in cancer initiation and tumor progression. Among all ECM proteins, we have focused on Emilin1, since it is able to impact on lymphangiogenesis, carcinogenesis and metastasis formation. However, Emilin1 role in the mammary gland development and in BC has not been fully elucidated. To fill this gap, we decided to study the phenotype of mice deriving from the intercross between the MMTV-Δ16HER2 transgenic animals and the Emilin1 knock-out (KO) ones. When mice were analyzed at prepubertal stage, before tumor onset, we observed that Δ16HER2/Emilin1KO mice displayed a macroscopic acceleration of mammary gland development. This result was also supported by specific investigation of key regulators of mammary gland plasticity, showing that while the ductal elongation/bifurcation stage was still ongoing at 11-weeks of age in female Δ16HER2/Emilin1WT animals, at the same age the KO counterpart was already going through a subsequent stage. When mice were analyzed at later time points, we observed that Δ16HER2/Emilin1KO mice displayed a significant anticipation of tumor onset (13.32 *vs* 15.28 weeks), even if accompanied by a tumor growth rate similar to that of wild-type littermates, suggesting a suppressive role for Emilin1 in tumor initiation. Consistent with the anticipated tumor onset, Δ16HER2/Emilin1KO mice displayed a higher number of tumor foci, both at 11 and 13 weeks of age, as evaluated by hematoxylin and eosin staining, immunofluorescence and western blot analysis. In addition, the dimensions of adipocytes were increased in the mammary glands of Δ16HER2/Emilin1KO background, suggesting a possible link between the anticipated tumor onset and the increased amount of adipose tissue.

Altogether, these results point to a role for Emilin1 in mammary gland development and in Δ16HER2-driven tumorigenesis, demonstrating the importance of this protein in mammary gland homeostasis and BREAST CANCER.

1. INTRODUCTION

1. INTRODUCTION

1.1 Breast cancer

Breast cancer (BC) is the most common cause of malignancy-related death in women worldwide, also representing the leading cause of cancer-related death. During the last years, BC incidence has risen in Northern and Eastern European countries, while remaining stable in several others. On the contrary, the incidence in Southern European countries displayed a decline. Since 1990s BC displays a favorable mortality trend thanks to the population screening, early diagnosis and improvement of therapies (Malvezzi et al., 2019; Carioli et al., 2020; Massat et al., 2016). As BC is a heterogeneous disease, many traits can be included as risk factors, like age, family history, early menarche and late menopause, some of which are modifiable factors, like post-menopausal obesity, use of combined estrogen and progestin menopausal hormones and breastfeeding. Lifestyle habits, such as diet, alcohol consumption and smoking, also account for modifiable factors (American Cancer Society, 2019-2020). In addition, nulliparity and late childbearing are well recognized risk factors of developing BC, because of hormonal perturbations causing an impact on mammary epithelial cell proliferation and cancer growth (Benson et al., 2009). The woman's cumulative lifetime exposure to estrogen determines the level of this environmental risk. Genetic predisposition also participates, accounting for approximately 10% of total BC cases in Western countries. The most relevant high-risk genes identified so far, BRCA1 and BRCA2, are both involved in biological processes like DNA repair and recombination, cell cycle control and transcription (McPherson et al., 2000; Venkitaraman et al., 2002). BRCA1 and BRCA2 effects are recessive, so both copies of an allele should be mutated or lost to promote cancer progression, but individuals carrying a germline mutation in these alleles have a dominant inherited susceptibility to BC since only a second hit mutation in the somatic allele is needed. However, BRCA1 and BRCA2 mutated mammary tumors are considered rare and do not explain the 10% of familial BC that is observed (Benson et al., 2009). Other genes that can play a role in BC susceptibility are *TP53, PTEN* and sometimes *H-RAS*. Interestingly, also mutations that can lead to other pathologies have been associated to increased risk of BC, as the heterozygous carriers of ataxia-teleangectasia (ATM) gene mutations and genes belonging to the Fanconi anemia pathway, which have been reported in 5% of familial mammary tumor cases (Antoniou et al., 2002; Melchor and Benitez, 2013).

Altogether, BC is a very common and heterogeneous pathology whose survival rates have been improved thanks to early diagnosis and increased number of available and effective therapies

(Richards et al., 1999). However, because of its molecular variability there is still the lack of a deep and complete knowledge of the pathogenesis, especially with respect to alterations, treatment sensitivity and cellular composition (Prat and Perou, 2010).

1.2 Breast cancer classification

Breast cancer complexity arises from the fact that it cannot be considered as a single disease, since it comprises many different biological entities which are responsible for distinct pathological features and clinical implications (Spitale et al., 2008; Desmedt et al., 2008; Sotiriou and Pusztai, 2009; Weigelt et al., 2010). The choice of the right therapeutic option must be based on the different histopathological and molecular features exhibited by the disease, which in turn lead to different treatment responses (Blows et al. 2010). First of all, BC can arise from different structures of the mammary gland; the ducts, the lobules and in some cases the tissue in between, further evolving with specific morphological features. The histological classification subdivides BC as reported below:

- **Invasive (infiltrating) carcinoma**, a heterogeneous group of tumors which comprehend infiltrating ductal, invasive lobular, ductal/lobular, medullary, tubular, mucinous and Paget disease. Among these, infiltrating duct carcinoma accounts for 70-80% of the cases, being the most common of the lesions (Malhotra et al., 2010; Li et al., 2005).
- **Non-invasive carcinoma or carcinoma *in situ***, which arises in the mammary ducts (DCIS) or lobules (LCIS) without invading the surrounding tissues, encompassing a heterogeneous group of tumors (Malhotra et al., 2010). Tumor architecture allows a further sub-classification of DCIS (more common than LCIS) into five well-recognized subtypes: Comedo, Cribiform, Micropapillary, Papillary and Solid (Bane et al., 2013).

Histological classification needs to be coupled with hormone receptor expression to better identify the characteristics and the behavior of the malignant lesion. For this reason, BC have been further sub-classified based on expression of estrogen and progesterone receptor and HER2/Erbb2 oncogene over-expression or amplification (Hergueta-Redondo et al., 2008). Based on these assessments, BCs can be further classified as follow:

- **Hormone Receptor-positive breast cancers (HR+ BC)** are characterized by estrogen (ER) and progesterone (PR) receptor expression. HR+ can be targeted by tamoxifen, an estrogen agonist able to inhibit the activation of estrogen receptor, which represents one of the first example of targeted therapies (Ali and Coombes, 2002; Higgins and Baselga,

2011), or by Fulvestrant, which inhibits the dimerization of ER and promotes its degradation (Carlson et al., 2005).

- **HER2-overexpressing breast cancers (HER2+ BC)** account for 15-20% of all BCs (Lamy et al., 2011). HER2 is a tyrosine kinase receptor-encoding gene that belongs to a family of transmembrane receptors which are activated by several extracellular ligands responsible for cell growth, differentiation and survival. While representing an unfavorable prognostic factor, HER2 represents a crucial predictor of response to anti-HER2 therapies, such as trastuzumab. After trastuzumab, several other HER2-targeted therapies have been developed in the last years, such as pertuzumab, neratinib and antibody-conjugates, such as T-DM1 and T-Dxd, commonly used as monotherapy or in combination, even with chemotherapy, to provide survival advantage to patients with HER2-overexpressing BC (Vogel et al., 2002).

- **Triple-negative breast cancers (TNBC)** lack the expression of ER, PR and do not display HER2 over-expression/amplification. TNBC is characterized by worse prognosis, tendency to relapse earlier and increased sensitivity to chemotherapy, in comparison to other subtypes (Dawood, 2010).

Finally, the progressive increase of knowledge regarding molecular alterations characterizing BC cells have allowed to improve BC taxonomy and to further group tumors based on the altered expression of specific set of genes, mainly through the development of dedicated cDNA microarray. In detail, 457 cDNA clones were selected among 8012 genes, to establish a starting classification. These genes were selected including those with the higher variation between different tumors, to better distinguish the inherent properties of the tumors themselves, rather than the differences arising from multiple sampling of the same tumor. The hierarchical clustering of these genes allowed the separation of tumors in different branches, each characterized by many cancer subtypes. The classification was based on the expression of genes related to the ER cluster, the ERBB2 amplicon at 17q22.24, keratins, laminins and genes expressed by the adipose tissue and non-epithelial cells (Perou et al., 2000; Sørlie et al., 2001). Evaluation of gene expression patterns that distinguish tumor subtypes seems to be a more reliable approach to stratify patient instead of single tumor marker analysis. Furthermore, the transcriptional program of tumor cells and their genetic alterations strongly impact on the tumorigenic potential and deeply influence the clinical outcome of the patient (Sørlie et al., 2003). From these studies, Perou and colleagues identified five intrinsic subtypes: luminal A, luminal B, basal-like, HER2-related and normal-like. More recently, also the claudin-low subtype has been identified (Prat et al., 2010).

1.2.1 Luminal subtype

Luminal BCs are tumors that originate from the cells that define the "lumen" of the ducts and lobules of the mammary gland. These luminal cells, and the derivative tumors, are characterized by the expression of estrogen receptor and estrogen-related genes. Based on gene expression profiling, breast tumors of the luminal subtype can be further divided in two subgroups, the luminal A and luminal B biological subtypes. Luminal A tumors usually show a lower expression of HER2-cluster genes and have a tendency to be less proliferative than the luminal B counterpart, displaying a low expression of Ki-67 (<20%) and other proliferative markers (Sørlie et al., 2001; Sørlie et al., 2003). Luminal B tumors display a higher proliferative rate (Ki-67 >20%) a higher frequency of TP53 mutations (Jacquemier et al., 2009) and, overall, a worse prognosis (Cheang et al., 2009). In general, the gene expression pattern of luminal BC subtypes closely resembles the one of the luminal epithelial cells of the mammary gland, displaying high levels of both luminal cytokeratin 8 and 18. Moreover, they show also the expression of four transcription factors as ER, GATA3, FOXA1 and XBP1 (Perou and Dale, 2011). GATA3 is recognized as a key regulator of mammary gland morphogenesis and luminal cell differentiation (Asselin-Labat et al., 2007); FOXA1 is a known downstream target of GATA3 and it is involved in the induction of numerous ER-regulated genes (Kouros-Mehr et al., 2006); XBP1 has an important role in the lactation phase where it takes part in the regulation of mammary epithelial cell expansion and in the development of an elaborated endoplasmic reticulum compartment (Davis et al., 2016).

1.2.2 HER2-enriched subtype

Genomic amplification of HER2 together with the overexpression of multiple HER2-amplicon-associated genes define the HER2-positive BC subtype. HER2-enriched breast tumors are further divided in two groups based on the estrogen receptor status: the HER2+/ER+ and the HER2+/ER- groups. The first one can also be progesterone receptor positive, being closer to luminal tumors and, for this reason, belongs to the luminal B intrinsic subtype (Carey et al., 2006). HER2-enriched cancers are frequently high-grade tumors and represent the 15-25% of all BCs (Perou and Dale, 2011), with the HER2+/ER+ group that displays a significantly better survival rate than the HER2/ER- group (Parise et al., 2009). As already discussed above, HER2+ tumors benefit from anti-HER2 targeted therapy. In particular, introduction of trastuzumab treatment in the early 2000s has greatly improved the natural history of these tumors and the overall survival rates of the patients, increasing the efficacy of first-line chemotherapy (Slamon et al., 2001).

1.2.3 Basal-like subtype

The basal-like subtype is thought to originate from the layer of basal epithelial cells of the mammary gland. This group of tumors is very often associated with triple-negative BC, according to immunohistochemical classification, since basal-like tumors are usually negative for hormone receptors and HER2 amplification. However, not all basal-like cancers are TNBCs and not all TNBCs are basal-like tumors (Perou and Dale, 2011). This subtype is characterized by the expression of genes peculiar of the basal epithelial cells, like cytokeratin 5, 6, 14, 17, vimentin and P-cadherin. Moreover, several of the genes overexpressed in basal-like tumors play a role in cell proliferation (MEK, ERK, PI3K, AKT, NF-kB, CCNE1, c-kit and EGFR), suppression of apoptosis, cell migration and invasion. Taken together, these genes contribute to an aggressive phenotype and a decreased cell differentiation. As mentioned, ER expression is reduced or absent, as well as that of several ER-responsive genes, more typical of the luminal compartment. HER2 overexpression is rarely found (Rakha et al., 2008). *TP53* mutations are frequent (80%) and the loss of *RB1* and *BRCA1* represent additional basal-like features (The Cancer Genome Atlas Network, 2012). Interestingly, the great part of *BRCA1* mutation carriers display basal-like cancers (80-90%) while only 15% is represented by sporadic basal-like tumors, wild type for *BRCA1* gene.

1.2.4 Claudin-low subtype

Claudin-low subtype was identified for the first time by the work of Prat and colleagues, in which they described a BC subtype characterized by low expression of different epithelial cell-cell adhesion molecules, like claudin 3, 4 and 7, occludin and E-cadherin. Claudin-low neoplastic lesions display high mesenchymal features and low epithelial differentiation. In fact, they show high expression of vimentin, N-cadherin, Snail1 and 2, Twist1 and 2, Zeb1 and 2 and HIF-1α (Prat et al., 2010). Many of these genes are frequently upregulated in cancer cells, conferring motility, invasiveness and leading to the activation of epithelial-to-mesenchymal transition (EMT). The EMT process increases the tendency of cells to disseminate, it is associated with chemotherapy resistance and it also increases the self-renewal properties (Mani et al., 2008). These self-renewal properties are peculiar of the tumor-initiating cells (TIC), a cellular subpopulation characterized by the expression of $CD44^{+}/CD24^{-/low}$ which is particularly enriched in the claudin-low subtype. Overall, these claudin-low tumors are mostly negative for ER, PR and HER2. Moreover, they display a high stromal infiltration, and this feature, together with the enhanced activation of the EMT program, might represent feasible therapeutic target (Fougner et al., 2020). Recent studies further classified the

claudin-low type into three more subtypes, identified the recurrent activation or the RAS-MAPK pathway, and hypothesized a basal origin for this type of cancer (Pommier et al., 2020).

1.3 The mammary gland

As mentioned above, the different subtypes of BC arise from different mammary epithelial cells, which are very tightly organized at hierarchical level. Thus, the study of the normal mammary gland has greatly improved the understanding of the different subtypes of BC, even shedding light on the molecular mechanism that characterize each of them. In fact, each of the altered pathways and mechanisms observed during tumor progression resemble those observed during normal mammary gland development and tissue remodeling (Visvader et al., 2009). The normal development of the mammary gland (MG) is a multistep process that occurs mainly after birth under the influence of hormonal fluctuation, involving many different signaling pathways with distinct regulatory functions and rules. The MG is a very complex tissue in which different cell types proliferate, differentiate and undergo apoptosis, provoking important changes in the global gland architecture and morphology, during the different phases of MG evolution. Among the different cells types that compose the MG, a restricted subpopulation of mammary stem cells fuels the dramatic changes showed by the MG during pregnancy. However, not only cell autonomous factors contribute to the MG remodeling, but also non cell autonomous ones, such as the extracellular matrix and cell-cell interactions, which deeply influence cell fate and function. Two main tissue compartments compose the mammary gland architecture: the epithelium and the stroma. The ducts and the alveoli, which display a central lumen that opens to the body surface through the nipple, constitute the epithelial compartment. Luminal and secretory cells represent the major part of the epithelial compartment; they differentiate during pregnancy to produce milk, whose delivery is ensued by a contractile compartment constituted by a system of basal and myoepithelial cells. All these structures are embedded in the stromal tissue, which is composed by adipocytes, fibroblasts, immune cells and cells belonging to the hematopoietic system. The mammary stem cells (MSCs), which are both able to self-renew and to differentiate into epithelial precursor cells (EPCs), are commonly proposed as the cells that give rise to the epithelial compartment (Figure 1). Once the EPCs are generated by mammary stem cells, they become restricted to a ductal or alveolar differentiation. On one hand, ductal precursor cells (DPCs) differentiate into basal or luminal cells, which in turn generate the ducts. The ductal structure is organized in two layers: the apically oriented layer and the basally oriented layer made by luminal epithelial cells and contractile basal myoepithelial cells, respectively. The expression of keratin 5, keratin 14 and smooth muscle actin characterize basal myoepithelial cells, which are in close

association with the basement membrane, whereas luminal cells express keratin 8 and keratin 18. On the other hand, alveolar precursors (APs) generate the alveoli during pregnancy, which dramatically changes the mammary gland architecture. Moreover, also basal and luminal cells are generated by APs. Luminal cells undergo a further step of differentiation into milk-producing cells, which are able to synthetize and secrete milk components thanks to the contraction of basal myoepithelial layer. Once the suckling process is stopped, mammary gland undergoes a massive remodeling celled involution. This process is achieved through alveolar epithelium apoptosis and restores a ductal system containing multipotent and committed ductal and luminal precursors (Henninghausen and Robinson, 2005).

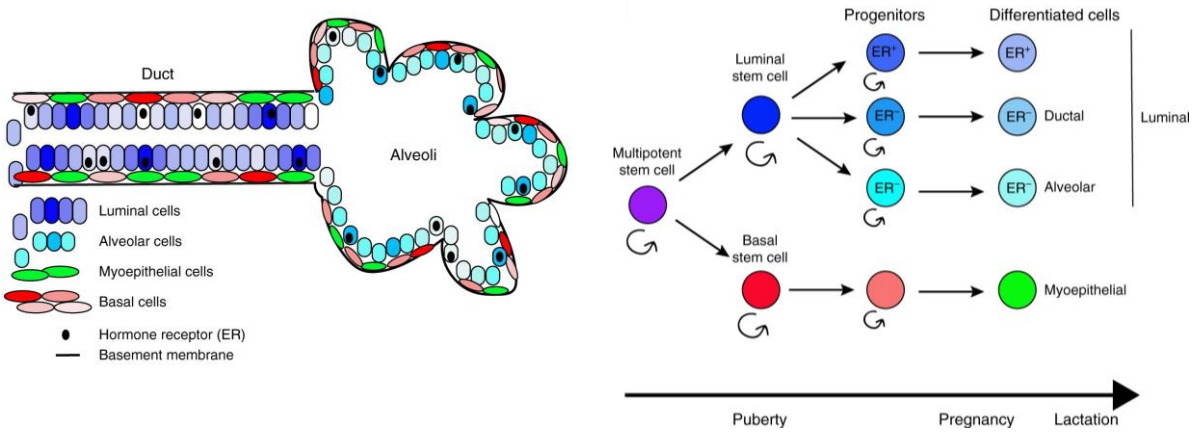

Figure 1. Dissecting the mammary gland one cell at a time (Crystea and Polyak, 2018)

1.3.1 Postnatal development of the mammary gland

Mice have been extensively used as a model to study the postnatal development of the mammary gland. After embryonic and prepubertal stage, hormones and other factors drive the additional changes. During pubertal stage the branching morphogenesis takes place, with the ductal epithelium of mammary primordium that invades the murine stroma, also called mammary fat pad (Figure 2). At the tips of growing ducts, club-shaped structures named terminal end buds (TEBs) drive the invasion of the mammary fat pad. These epithelial structures are highly proliferative and invasive, sharing also some features with mesenchymal cells, suggesting that a sort of epithelial to mesenchymal transition takes place in these sites. TEBs are made of two different cell types: cap cells line the end of the bud,

forming the cap of the structure and keeping the contact with the surrounding stroma, apparently differentiating into myoepithelial basal cells; body cells constitute the inner layer of the end bud, with the central body cells that undergo apoptosis to form the lumen of the duct and the remaining cells that differentiate into luminal epithelial cells. These cells will generate the ductal epithelium of the adult mammary gland. TGF-β pathway plays an important role in the branching step, in fact its activation stops the branching process once the mammary fat pad is filled. During this step, TGF-β pathway seems to be regulated by mechanical and local cues, provided by the gland architecture (Nelson et al., 2006; Inman et al., 2015). Mammary gland architecture of virgin mice is remodeled during each estrus cycle by a fine-tuned loop of proliferation and apoptosis of the epithelium. Further development and remodeling are present during pregnancy, when the mammary gland has to prepare for lactation. These additional changes are needed to generate cells able to produce a large quantity of milk and are mainly influenced by two hormones, progesterone and prolactin. Progesterone mainly induces an extensive side-branching and alveologenesis, whereas prolactin promotes the differentiation of mature alveoli. The drastic increase in side- and tertiary-branching is the first remodeling step taking place during pregnancy, providing ductal arbors for the next transformation, *i.e.* the alveolar development. Proliferating epithelial cells generate the alveolar buds, which then cleave and differentiate into distinct alveoli, further becoming milk-secreting lobules during lactation. The proliferation of epithelial cells progressively populates inter-ductal spaces, reducing the area occupied by interstitial adipose tissue.

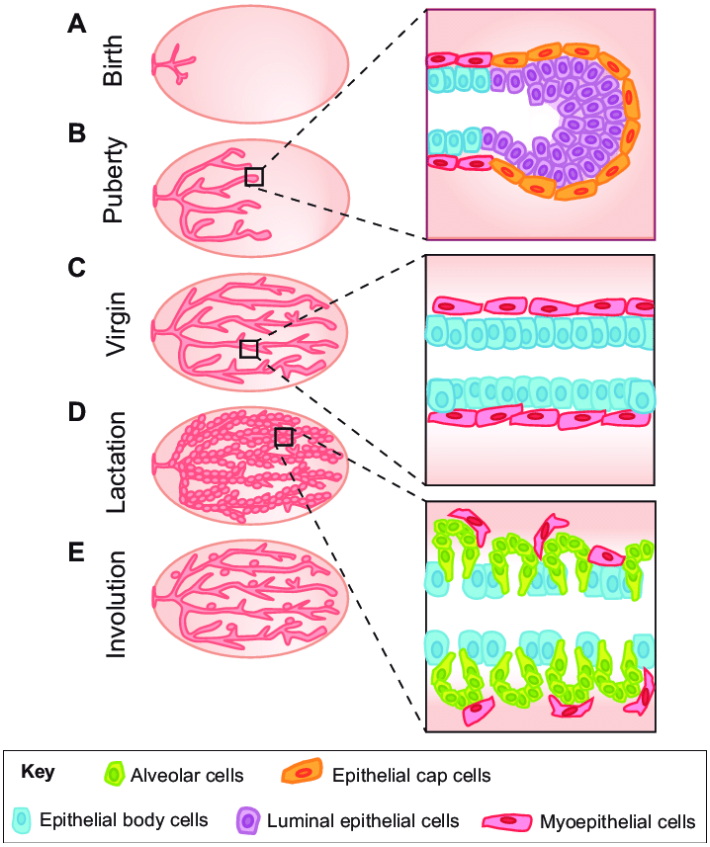

Figure 2. The branching morphogenesis of mammary gland (Inman et al., 2015)

1.3.2 Transcriptional regulators of mammary gland development

The regulation of postnatal mammary gland development is a complex interplay of hormones and paracrine factors, whereas embryonic mammary gland morphogenesis is still poorly characterized. Estrogen, progesterone and prolactin are the main actors during puberty, pregnancy and lactation, underlining the importance of steroid and peptide hormones in the gland architecture (Figure 3). Estrogen is an ovarian hormone, and it is the principal regulator of pubertal stage. During this step, estrogen receptor-α (ER-α) is the main regulator of branching process, whereas progesterone and progesterone receptor (PgR) are mainly involved in adult tertiary side branching. Moreover, also the crosstalk between developing duct epithelium and stromal cells takes part in organizing the branching process. Esr1-depleted mice develop a rudimentary duct system that that fails to undergo the estrogen-mediated growth spurt that accompanies puberty. In addition, a role of Esr1 has been found during pregnancy in the maintenance of alveolar cells, with a defective development of lobuloalveolar compartment and inadequate milk production that arise after Esr1 depletion in alveoli following ductal elongation (Feng et al., 2007). Concerning PgR, it plays a minor role during dual branching,

instead it is one of the key regulators in the expansion of the alveolar compartment. Depletion of PgR in mice causes an impairment in ductal proliferation and alveolar differentiation, showing only the formation of a simple epithelial tree (Lydon et al., 1995; Brisken et al., 1998). Receptor Activator Nuclear factor kB-Ligand (RANK-L) is the mediator of PgR proliferative effect, with a proven role in the regulation of skeletal calcium release that is connected with alveologenesis regulation. In fact, this is the first step in maternal calcium transfer to infant mammals. Mice that lack RANK-L or its receptor RANK display similar phenotype to PgR-depleted mice, failing the process of alveologenesis during pregnancy (Fata et al., 2000). Another key player in mammary gland remodeling is E74-like factor 5 (Elf5), which has been proposed as Prl/Jak2/Stat5 axis regulator, taking part in cell differentiation, alveologenesis and lactogenesis. Homozygous lack of Elf5 in mice is lethal very early during embryogenesis, whereas heterozygous Elf5 deletion in mice females provokes an impaired mammary alveolar morphogenesis. The main actor in lactogenesis during pregnancy is prolactin (Prl), which acts through its downstream intracellular partners Janus kinase-2 (Jak2) and Signal Transducer and Activator of Transcription 5 (Stat5). Prl acts both directly on the mammary epithelium and indirectly regulating progesterone production. The binding with its receptor (PrlR), prolactin causes the dimerization of the receptor, further recruiting Jak2, which in turns phosphorylates PrlR. Jak2 subsequently recruits and phosphorylates Stat5, which subsequently translocates in the nucleus to activate genes necessary for cell proliferation and expression of milk proteins (Henninghausen and Robinson, 2005). Inactivation of PrlR alleles in female mice does not affect ductal outgrowth during puberty, but strikingly no functional alveolar compartment was formed during pregnancy. As a consequence, these mice cannot maintain pregnancies. Heterozygous deletion of PrlR causes a block in proliferation and differentiation during the second half of pregnancy (Ormandy et al., 1997; Brisken et al., 1999; Gallego et al., 2001). The PrlR/Jak2/Stat5 axis activates the transcription of milk protein genes, like β-casein (Csn2) and whey acidic protein (Wap).

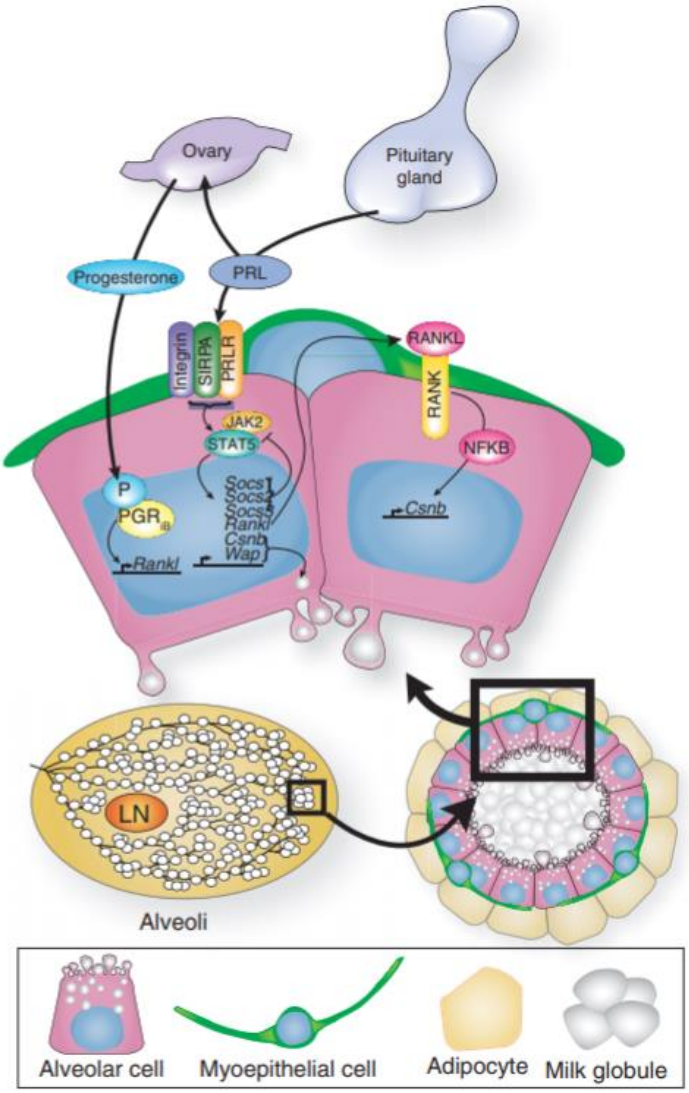

Figure 3. Schematic view of the events that generate lactation competence during pregnancy (Macias and Hink, 2012)

1.4 The ErbB/HER family of protein-tyrosine kinases

Another family of kinases that plays a very important role during mammary gland development is the HER/ErbB family. The Human Epidermal Receptor (HER) family of receptor tyrosine kinases (RTKs), also known as ErbB is composed by four members: EGFR (ErbB1, HER1), HER2 (ErbB2, HER2/neu), HER3 (ErbB3) and HER4 (ErbB4) (Figure 4). They are typical RTKs which can be bound by at least 12 known EGF-like peptides further subdivided in three groups based on receptor specificity (Hynes and McDonald, 2009). The signaling cascade is initiated by ligand binding, which in turns stimulate the specific dimerization between two identical (homodimerization) or different (heterodimerization) receptors belonging of the family (Moasser, 2007). The dimerization starts the intrinsic kinase activity and causes the phosphorylation of specific C-terminal tyrosines, providing

the docking sites for proteins carrying the Src holomogy 2 (SH2) or phosphotyrosine binding (PTB) domains (Olayioye et al., 2000). The autophosphorylation pattern of the C-terminal region is specific for each receptor of the family. Several pathways are stimulated by ErbB signaling, like the mitogen activated protein kinase (MAPK) pathway or the phosphatidylinosithol-3-kinase (PI3K) pathway, leading to the regulation of cell-cycle progression. In a general view, transcriptions factors localized downstream the HER pathway are involved in cell proliferation, cell survival, adhesion, migration, cell polarity and differentiation (Holbro and Hynes, 2004). More in detail, ErbB2/HER2 is necessary during the early stages of ductal outgrowth through a cell-autonomous mechanism, whereas HER1/EGFR and ErbB4/HER4 are involved in growth and differentiation of mammary gland and during pregnancy. ErbB2/HER2 levels are tightly regulated: while low levels during puberty result in a delayed ductal outgrowth, elevated expression is associated to very aggressive human BC. Mice lacking *ERBB2* show mammary buds which slowly advance through the mammary fat pad, exhibiting a defect in penetration. This phenotype perfectly matches the aggressiveness of mammary tumors that exhibit *ERBB2* amplification (Andrechek et al., 2005; Jackson-Fisher et al., 2004). Moreover, terminal end buds of these mice display structural defects, with decreased body cells number, increased cap-like cells number in the pre-luminal compartment and the presence of large luminal spaces. HER1/EGFR and ErbB4/HER4 are also involved in mammary gland remodeling regulating growth and differentiation, as well as during pregnancy. HER2 and EGFR co-localize in many mammary gland compartments at puberty. Instead, after puberty HER2 is prominent in the epithelium and reduced in the stroma, while EGFR is localized in the stromal cells around the TEB. Moreover, EGFR ligands are believed to mediate the effect of steroid hormone in the mammary gland through local regulation of mammary gland growth and development via stromal-epithelial interactions (Parmar and Cunha, 2004). On the other hand, HER4 is more localized in the ducts, playing a fundamental role especially in late pregnancy and lactation, exhibiting a strong phosphorylation. Depletion of HER4 in the mammary epithelial cells leads to an impaired activation of STAT5, impacting on alveolar differentiation and lactation (Hynes and Watson, 2010). As widely reported in literature, this family of RTKs is deeply involved both in normal physiology and cancer, in which they are often found mutated or amplified (Mishra et al., 2017).

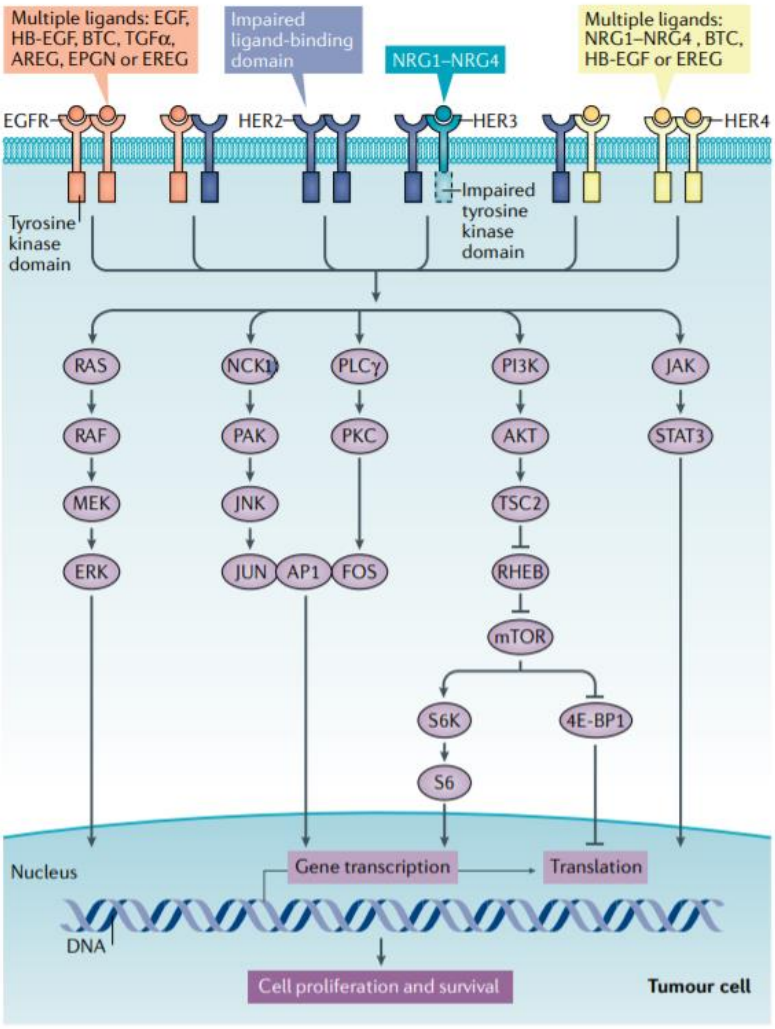

Figure 4. Signaling pathways activated by ERBB family members (Kumagai et al., 2021)

1.4.1 The HER2 oncogene and its splice variants

The first description of HER2 dates back to 1980s from rodent models and humans. ErbB2 is used both for human and rodent gene. HER2 and *Neu* refers to human and rodent gene, respectively. Two ligand-binding regions (LD1, LD2) and two cysteine-rich regions (CR1, CR2) constitute the extracellular domain of HER2, which is connected to a short transmembrane domain followed by the intracellular kinase domain. Differently from the other members of the family, HER2 extracellular domain lacks a high-affinity ligand, existing as an open and constitutively active conformation. This characteristic renders HER2 the preferred heterodimerization partner of all other ErbB ligand-bounded receptors (Moasser, 2007). HER2 is usually described as a proto-oncogene and its overexpression is present in approximately 20% of BC, conferring a more aggressive phenotype. The amplification of HER2 gene can reach 25-50 copies in BC, with a fold increase of the relative protein

up to 40-100. HER2 amplification is recognized as an early event in BC pathogenesis, and its status is kept throughout the progression to invasive disease, nodal and distal metastases (Perou et al., 2000; Tsuda et al.,2001). The process of HER2-mediated tumorigenesis is complex, and even if many informations have been collected during the past years, still a unique model of transformation has not been described. Up to now, two different mechanisms have been recognized to explain the mammary epithelial cell transformation induced by HER2: the first involves an increased kinase activity and over-phosphorylation of itself and cellular substrates, whereas the second relies on the increased expression of HER2 and its splice variants, in particular the rare Δ16HER2 isoform. In literature, three naturally occurring splice variants of HER2 are described: p100 (100 kDa), Herstatin and Δ16HER2 (Figure 5). p100 mRNA encodes for the first 633 amino acids of the extracellular domain of the full-length protein, it is a soluble form of the receptor that is able to interfere with the oncogenic activity of the wild-type HER2. The intron 15 retention generates an in-frame stop codon responsible for this splice variant, which shows a decreased downstream activity of the MAP kinase pathway and the inhibition of tumor cell proliferation (Sasso et al., 2011). Herstatin is also a soluble splice variant, which arises from intron 8 retention during the mRNA processing. This 68 kDa truncated form comprises the extracellular domain 1 (ECD1) and most of extracellular domain 2 (ECD2) of HER2, followed by a peculiar C-terminus. Herstatin acts as a negative regulator of HER2 disrupting dimers, decreasing tyrosine phosphorylation further inhibiting the growth of HER2 overexpressing cells. Due to its abilities, it has been described as a growth regulator during normal development (Koletsa et al., 2008). The third splice variant, named Δ16HER2, arises from an in-frame deletion of exon 16 and lacks the expression of 16 amino acids in the juxtamembrane domain. Skipping of exon 16 results in the loss of two cysteine residues that participate in intramolecular bonding, leaving the remaining cysteines available for intermolecular interactions. These intermolecular disulphide-bridges leads to homodimerization and constitutive activation of Δ16HER2 receptor (Castiglioni et al., 2006). Δ16HER2 splice variants represents only the 4-9% of total HER2 transcripts, but it is co-expressed in the great part of HER2-positive breast tumors, possibly playing a critical role in the activation of many oncogenic pathways in these tumors. Moreover, literature describes the cooperation between Δ16HER2 and Src kinase, a common mechanism associated with trastuzumab resistance (Zhang et al., 2011). Src has found to co-localize with Δ16HER2 at the cell membrane, physically interacting with the aberrant protein in HER2-overexpressing breast tumors. In addition, Src is a well-known activator of many oncogenic pathways like FAK, PI3K and MAP kinase, regulating mainly cell motility and invasion (Mitra et al., 2009). It has been demonstrated that the presence of Δ16HER2 variant is necessary and sufficient to lead the oncogenic transformation of immortalized mammary epithelial cell lines due to an impaired downregulation from the cell surface. In fact, while activated

HER2 is rapidly degraded, no endosomal detection of Δ16HER2 has been reported (Turpin et al., 2016). The relation between Δ16HER2 and the response to trastuzumab is still debated. On one side, *in vitro* evidences highlight the importance of Δ16HER2 expression as an important step in driving trastuzumab-refractory BC (Mitra et al., 2009), on the other a recent work demonstrated the efficacy of trastuzumab treatment in impairing the spontaneous tumor growth in transgenic mice overexpressing Δ16HER2 (Castagnoli et al., 2014).

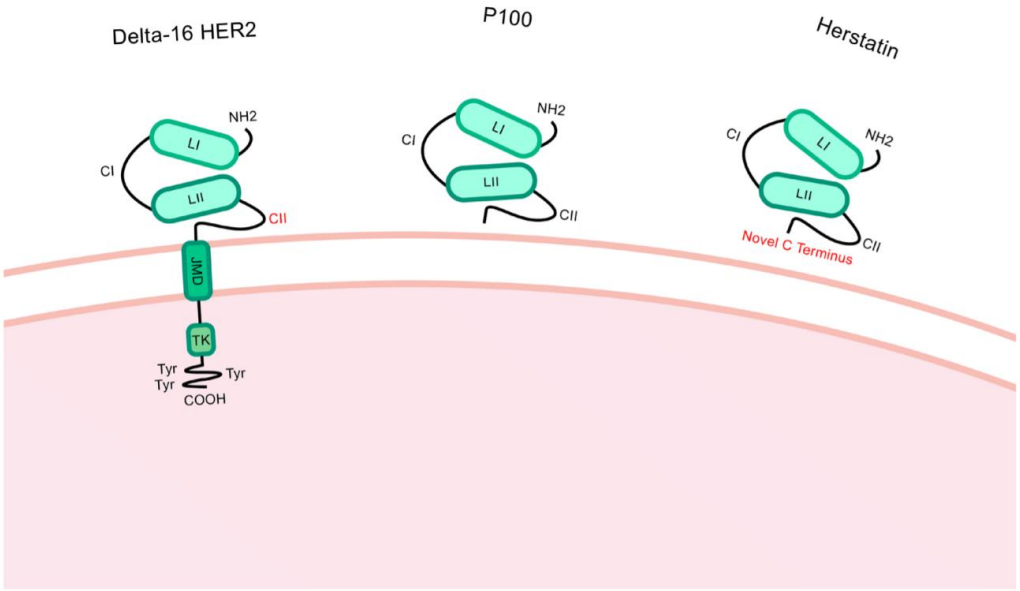

Figure 5: Structure of Δ16-HER2, P100 and Herstatin splice variants (Hart et al., 2020)

1.5 Δ16HER2 transgenic mouse model

Murine models based on the mouse mammary tumor virus (MMTV) promoter have been widely used to better investigate the mechanisms involved in HER2 tumorigenesis. The first model was designed in 1988 by Muller and colleagues, and it was characterized by the development of mammary tumors due to activated neu (neu-NT) expression, driven by the MMTV promoter (Muller et al., 1988). This mouse exhibited fast onset (11-13 weeks) and the development of a high number of tumor masses, leading to the hypothesis that the overexpression of neu-NT was able to start breast carcinogenesis in a single step. However, it is known that the random insertion of the transgene can impinge on the phenotype, in fact one year later a similar murine model was generated and it exhibited longer latency,

probably due to different insertion of the transgene in the mouse genome, leading to altered transgene expression (Bouchard et al., 1989). Nevertheless, further studies confirmed the ability of activated neu to induce a single-step tumorigenesis (Guy et al., 1996; Moody et al., 2002). However, this mutation has never been found in patients, so the following works focused the attention on the overexpression of wild-type HER2, to closely resemble the clinical situation. Different attempts to generate the wild-type HER2 model were made, with different results. A transgenic murine model with the whey acidic protein promoter-driven expression of HER2 was generated, however no tumor onset was observed (Piechocki et al., 2003). Conversely, a model with MMTV-driven expression of HER2 displayed a late tumor onset (Finkle et al., 2004). An important finding came from the sequencing of human HER2 transcripts of these models, highlighting the presence of an in-frame deletion of 15-bp inside the HER2 juxtamembrane domain, which affects the cysteine-mediated dimerization (Finkle et al., 2004). To better investigate this deletion, a transgenic murine model expressing the Δ16HER2 splice variant was generated in 2011 (Marchini et al., 2011). Taking advantage from the specificity of the MMTV promoter, which is hormone-regulated, an expression cassette containing the human Δ16HER2 gene has been inserted under its control, thus driving the expression mainly in the mammary gland (Figure 6). The chromosome 5 is the site of a single insertion of the transgene, in an intergenic region lacking genes and regulatory sequences. Moreover, the transgene is located far from two genes positioned downstream and upstream the insertion site, thus ensuring that the insertion itself does not affect the tumorigenesis. As expected, the analysis of human HER2 transcripts extracted from murine mammary primary tumors revealed and in-frame 15bp deletion in the wild-type juxtamembrane region, which seems necessary to start the malignant transformation. Also in this case, the deletion leads to reposition of the cysteines, thereby affecting the cysteine-mediated receptor dimerization. Collectively, these data support the hypothesis that Δ16HER2 protein might be a very critical mediator of HER2 tumorigenesis. Accordingly, Δ16HER2 mice shows higher tumor incidence, faster tumor growth rate and shorter latency period, in comparison with wild-type human HER2-overexpressing mouse models (Marchini et al., 2013). The 100% malignant transformation in Δ16HER2 mice is guaranteed with only five copies of the transgene, whereas 30-50 copies of HER2 human transgene are needed to induce oncogenesis, and only in 80% of MMTV-wild-type hHER2 transgenic mice (Marchini et al., 2013). Moreover, Δ16HER2 transgenic females exceed MMTV-wild-type hHER2 mice both in average latency of tumor development (only 15.11±2.5 weeks vs. 28.6 weeks) and in number of tumor masses. The aggressiveness of Δ16HER2 mouse model is also confirmed by development of lung metastases, starting approximately from 25 weeks of age. The origin of these lung metastases is confirmed by their HER2 robust positive staining (Marchini et al., 2011). Looking at all these data, it is clear that

WT hHER2 expression is not sufficient "*per se*" to drive malignant transformation, while the Δ16HER2 splice variants is able to drive the oncogenic transformation alone *in vivo*.

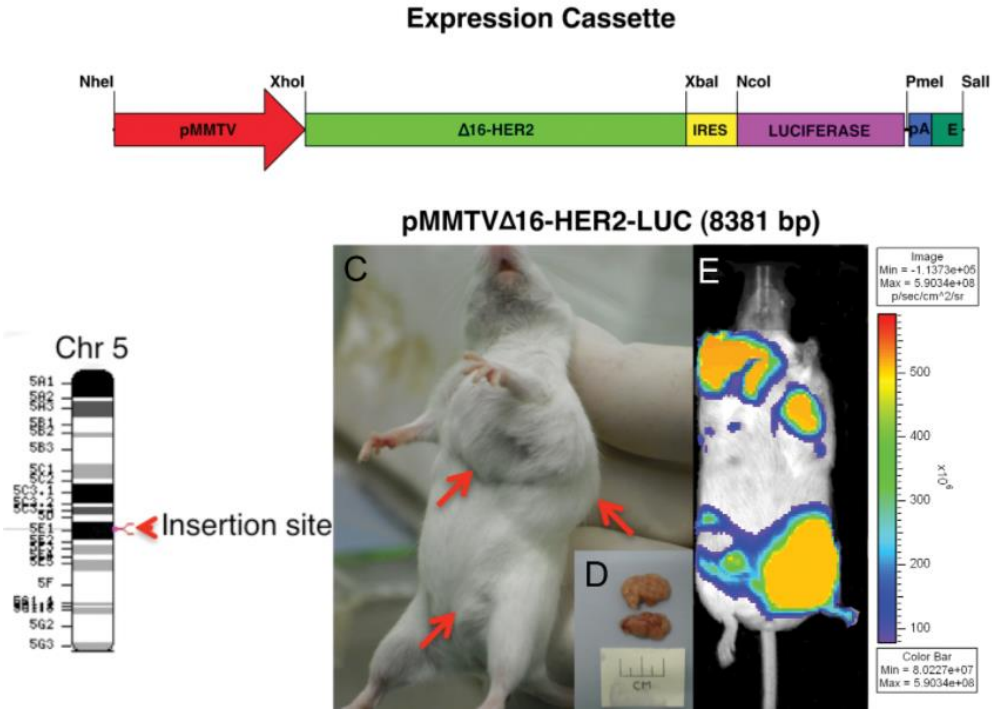

Figure 6. Δ16HER2 transgenic mice develop spontaneous multiple mammary tumors (Marchini et al., 2011)

1.6 The extracellular matrix in tumorigenesis

The extracellular matrix (ECM) is probably the component of the tumor microenvironment (TME) that has been less investigated. However, its importance has gained attention over the last decade. Many ECM molecules have been found enriched in solid tumors (fibrillary collagens, fibronectin, elastin and laminins) reaching up to 60% of the composition of the tumor mass. These molecules are produced both by tumor cells and by cancer-associated fibroblast (CAFs), resulting in a disorganized accumulation of ECM components which is associated to poor prognosis and resistance to chemotherapy. CAFs contribute also secreting paracrine factors that support tumor cells, like stromal cell-derived factor-1 (SDF1) and transforming growth factor beta (TGF-β) (Wang et al., 2021; Yu et al., 2013). TGF-β is one of the key regulator of the epithelial to mesenchymal transition (EMT), which is a fundamental process during tumorigenesis (Xu et al., 2009) and allows an epithelial, well-polarized cell to undergo a rearrangement toward a mesenchymal phenotype, increasing its migratory ability, invasiveness, resistance to apoptosis and strongly enhancing the production of ECM molecules (Kalluri et al., 2003; Kalluri et al., 2009). The ECM fraction of the TME can strongly

diverge from the heathy tissue, both in terms of amount of deposition, composition, organization and post-translational modification of its proteins (Henke et al., 2020). Due to the importance of ECM variation in the TME, it has also been evaluated as prognostic factor. Bergamaschi and colleagues divided BC samples in four subgroups, according to their ECM expression profile that correlated strongly with prognosis (Bergamaschi et al., 2008). Moreover, the alteration of ECM structure and composition can negatively impact in the response to therapy. A stiffer matrix might behave as a shield for tumor cell clusters, protecting them from therapeutic agents and increasing hypoxia and metabolic stress, thus leading to the activation of anti-apoptotic and drug resistance pathways. The increased stiffness might modify also the response to chemotherapy, *via* integrin/FAK signaling. In general, it is known that during development and tumorigenesis, there is an increase in deposition and cross-linking of collagen as well as hyaluronan acid content, causing an increase in ECM stiffness (Levental et al., 2009; Gkretsi et al., 2018). Moreover, literature data report the evidence that the ECM stiffness is strongly implicated in cancer development (Bissell et al., 2011; Bonnans et al., 2014). Due to the importance of ECM in tumorigenesis, it is not surprising that an increasing number of clinical trials is including drugs that target ECM molecules (Henke et al., 2020). In BC patients, good results were obtained with the use of hyaluronidase in combination with erlotinib. In conclusion, approaching ECM as a putative target of therapy currently seems an appealing strategy. Many challenges still have to be mastered in this context, but a better knowledge of ECM-tumor interplay might significantly improve the performance of therapeutics that are already employed in the clinical setting (Henke et al., 2020).

1.7 Emilin1

Emilins (Elastic Microfibril Interface Located proteIN) and Multimerins together form a protein family that shares both the C-terminal gC1q domain, characteristic of the gC1q/TNF superfamily, and the EMI domain, located at the N-terminal portion of the protein, which has a homology of 60% to 70% between family members (Colombatti et al., 2000; Doliana et al., 2000; Colombatti et al., 2012). These glycoproteins of the ECM assemble into high molecular weight multimers and are involved in various functions, some of which are due to the gC1q domain, while others have not yet been assigned or linked to a specific region of the proteins (Colombatti et al., 2012). Emilin1 is an ECM glycoprotein and the founding member of the EDEN superfamily (Bressan et al., 1983). It was first isolated in heterogeneous fractions obtained from arteries of newborn chickens and was noticed for its peculiar distribution on the surface or amorphous elastin (Colombatti et al., 2000). Its structure can be mainly subdivided into five different domains: the N-terminal domain, called EMI domain;

the central coiled-coil region; the leucine zipper domain; the collagenous domain and the C-terminal gC1q domain (Figure 7).

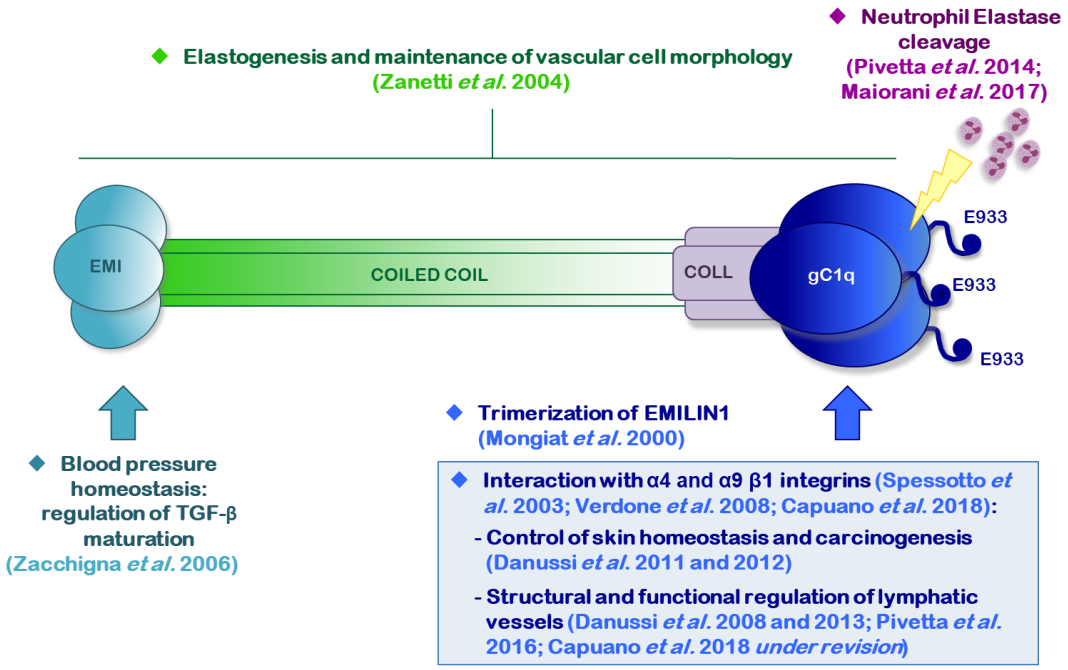

Figure 7. Summary of the functions ascribed to the different domains of Emilin1 (courtesy of Alessandra Capuano)

The N-terminal domain of Emilin1 is associated with the control of blood pressure homeostasis. Indeed, *Emilin1* knockout mice show increased blood pressure, higher peripheral vascular resistance and smaller vessel size in comparison to their wild-type littermates. Mechanistically, this phenotype results from binding between the N-terminal EMI domain and pro-TGF-β precursor, which prevents maturation of the cytokine by furine convertases in the extracellular space. Strong evidence is provided by genetic ablation of *Emilin1*, which enhances TGF-β signaling in the vascular wall. Moreover, a single inactivation of *TGF-β1* allele is able to rescue blood pressure parameters to normal levels (Zacchigna et al., 2006). The function of the central coiled-coil region remains to be elucidated. However, Iacomino and colleagues have recently identified a novel heterozygous *Emilin1* mutation that falls inside this domain, namely c.748C>T [p.R250C], which was observed in four affected members of a family exhibiting a distal motor neuropathy phenotype. Sensory nerve biopsies from these patients display unspecified changes in the number and morphology of myelinated fibers. In addition, skin biopsies and skin-derived fibroblasts show an altered pattern of Emilin1 deposition compared with healthy samples. *In vitro* experiments with zebrafish in which *emilin1a* was downregulated displayed developmental delay, movement defects and abnormal axonal branching of spinal cord motoneurons. Wild-type zebrafish *emilin1a* rescued the phenotype as well as partially by

human wild-type Emilin1 cRNA, but not by cRNA with the aforementioned mutation. All this evidence suggests a possible role for Emilin1 in the pathogenesis of peripheral nervous system diseases (Iacomino et al., 2020). The presence of a leucine-zipper domain is a rather rare case for an ECM protein. Only a few cases are known reported in the literature: an ECM protein from *Drosophila Melanogaster* called pollux (Zhang et al., 1996) and dystrophin, a cytoplasmic protein that can interact with troponin (Pearlman et al., 1994). The C-terminal gC1q domain is quite peculiar, containing only a nine-stranded β-sandwich fold instead of ten, with the last strand replaced by a disordered 19-residue-long segment. The gC1q domain has been identified as an important site for adhesion between Emilin1 and the cell surface integrins α4β1 and α9β1 (Spessotto et al., 2003). Moreover, the interaction between Emilin1 and α4β1 integrin downregulates MAPK pathway via HRAS leading to decreased proliferation in an epithelial system (Modica et al., 2017). Interestingly, this interaction could be affected by neutrophil elastase, which is able to cut the gC1q domain outside the E933 integrin binding site (Pivetta et al., 2014). The E933 residue is essential for the correct behavior of the gC1q domain.

1.8 The Emilin1 knockout and the Emilin1-E933A murine models

The generation of specific murine models strongly helped in unveiling and elucidating many Emilin1 functions. The Emilin1 knockout model was generated by inserting the *lacZ-pgk-neo* cassette into exon1 of chromosome 2p23.3 (Figure 8), truncating the coding sequence immediately downstream of the signal peptide. As a result, no functional domains of Emilin1 should be present in the translation product of the mutant gene. Both hetero- and homozygous animals for the mutation were fertile, had normal life expectancy and exhibited growth rate indistinguishable from wild-type littermates. (Zanetti et al., 2004).

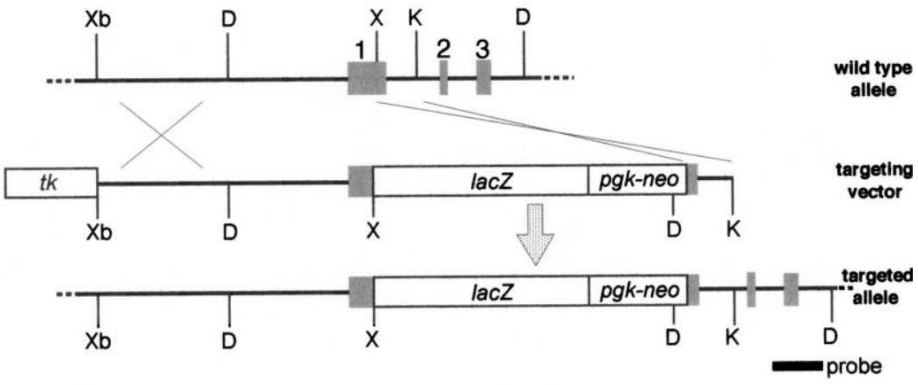

Figure 8. Generation of EMILIN-1-deficient mice (Zanetti et al., 2004)

Moreover, detailed examination showed alterations in the structure of elastic fibers and in cells that make up the arteries. As for lymphatic circulation, comparison between wild-type mice and Emilin1 knockout littermates showed hyperplasia, enlargement and an altered pattern of superficial and visceral lymphatic vessels in the knockout mice. In addition, these animals exhibited a reduced number of anchoring filaments. The structural defects are also associated with functional impairments. Thus, Emilin1 knockout mice have mild lymphedema, decreased lymphatic drainage and increased leakage (Danussi et al., 2008). Dermal and epidermal hyperproliferation was also observed (Danussi et al., 2011). In this work, Danussi and co-workers suggest that the interaction between Emilin1 and α4- and/or α9β1 integrins maintains the proliferative homeostasis in basal keratinocytes and dermal fibroblasts. Differently from the proproliferative signals that usually arise from ligand-activated integrins (Clark et al., 1995; Walker et al., 2005; Gilcrease et al., 2007; Streuli et al., 2009), the cues coming from Emilin1-ligated α4/α9 are antiproliferative. When exposed to chemical carcinogens, Emilin1 knockout mice show accelerated tumor formation, higher incidence, and development of a greater number of tumors compared to wild-type mice. Consistent with these data, the number of lymph nodal metastases number is also increased in knockout mice transplanted with syngeneic tumors. Moreover, *in vitro* migration studies showed enhanced transport of tumor cells in an Emilin1-depleted environment. All these data pinpoint a tumor suppressive role of Emilin1 in various contests (Danussi et al., 2012). Detailed studies were performed to better characterize the different domains of Emilin1. To better characterize the interaction of gC1q with α4 and α9β1 integrins, a new transgenic mouse model expressing E933A-mutated Emilin1 (E1-E933A) was generated. Mutation in this key residue impairs the interaction with integrins, and the mutant mice present altered lymphatic vessels architecture, showing a dense and tortuous network. In addition, the number of anchoring filaments is reduced in E1-E933A mice and collectors' valves exhibit an aberrant and narrowed structure. Lymphatic circulation function is also impaired, with mutant mice being more susceptible to lymph node metastasis (Capuano et al., 2019). Treatment of Emilin1 knockout mice with AOM-DSS (Azoxymethane-Dextran sodium sulfate), a widely used initiation-promotion model that employs the chemical induction of DNA damage followed by several cycles of colitis (Tanaka et al., 2003; Suzuki et al., 2005) resulted in higher tumor incidence, larger adenomas and lower survival compared to wild-type animals. E1-E933A mice showed similar results. Moreover, chronic treatment with DSS in both mouse models resulted in increased inflammatory infiltrates, higher colitis score and stronger mucosal injury respect to wild-type littermates. In conclusion, ablation of Emilin1 may lead to a reduction in inflammatory resolution during colon cancer progression, due to decreased lymph flow and inefficient clearance of inflammatory cells (Capuano et al., 2019).

2. AIMS

2. AIMS

Breast cancer is the most common cause of cancer-related death in women worldwide. This trend persists even with the increased efficiency of the screening campaign, that leads to early diagnoses, and with the introduction of new targeted therapy. One of the main problems is represented by the heterogeneity of the disease, which renders not entirely predictable the patient response to treatments. HER2 positive BC accounts for 15-20% of all BC and it is frequently associated to poor prognosis. The Δ16HER2 splicing variant, which is characterized by the deletion of exon 16, leads to an increased oncogenic ability in comparison to the wild-type form, represents the 4-9% of total HER2 transcripts. The extracellular matrix (ECM) is a key component of the tumor microenvironment, acting as growth factors reservoir that are used by the tumor to sustain growth and progression. Emilin1 is an ECM protein member of the Emilin/Multimerin family and it has proven roles in lymphangiogenesis, carcinogenesis and metastatic spreading of tumor cells. In this PhD project we aim to investigate how the loss of Emilin1 expression impacts on mammary gland development and in Δ16HER2-driven tumorigenesis. To pursue these aims we generated the FVB Δ16HER2/Emilin1 knock-out mouse model. First, we characterized mammary gland development, analyzing the morphology and investigating key regulators of its development, looking at the adipocytes content of the tissue and evaluating the elastic fibers deposition around the milky ducts. Then, we investigated the mammary tumor onset and progression at different time points of tumor growth and metastatic dissemination. Finally, to better investigate metastatic spreading, we took advantage of syngeneic injection of EO771E2 HER2+ BC cells in C57BL/6 mice, looking at nodal metastases.

3. RESULTS

3. RESULTS

3.1 Generation of the FVB MMTV-Δ16HER2/Emilin1KO mouse model and characterization of the mammary gland architecture

It is well known that the extracellular matrix (ECM) plays a fundamental role in tumor initiation and progression, particularly in BC. Among other components, Emilin1 has been involved in tumor cells proliferation, migration and lymph node invasion (Danussi et al., 2012; Qi et al., 2019). We thus decided to investigate whether loss of Emilin1 could play a role in the context of BC. To do so, we took advantage of the MMTV-Δ16HER2 transgenic model, a murine model of BC which displays very aggressive features, in which transgenic females spontaneously develop multifocal mammary tumors starting from 15 weeks of age (Marchini et al. 2011). After an initial characterization that confirmed that our colony shared the same features of the one from the original work (average onset at 15.28 weeks), we generated the FVB MMTV-Δ16HER2/Emilin1 knockout (KO) mouse model intercrossing Δ16HER2 males with FVB Emilin1KO females, from our already established colony (Zanetti et al., 2004). First, we wondered whether the ablation of Emilin1 could impact on the normal murine mammary gland (MMG) structure and/or function, due to its peculiar association with the elastic fibers and with the lymphatic vasculature. Thus, using immunofluorescence staining, we analyzed the conformation of the normal MMG of Emilin1 WT and KO mice and then looked at Emilin1 deposition in those MMG (Figure 1A) and in glands bearing tumor foci (Figure 1B). As it is possible to see from the staining with the cytokeratins, the MMG architecture of Emilin1 KO mice was quite similar to the WT one and did not present any evident defect (Figure 1C). Emilin1 was clearly deposited in the ECM surrounding and sustaining the mammary ducts and the tumor mass, while it was not present inside the tumor. This peculiar deposition could be involved in the maintenance of mammary gland architecture, suggesting that its loss could impinge in different steps of mammary tumorigenesis.

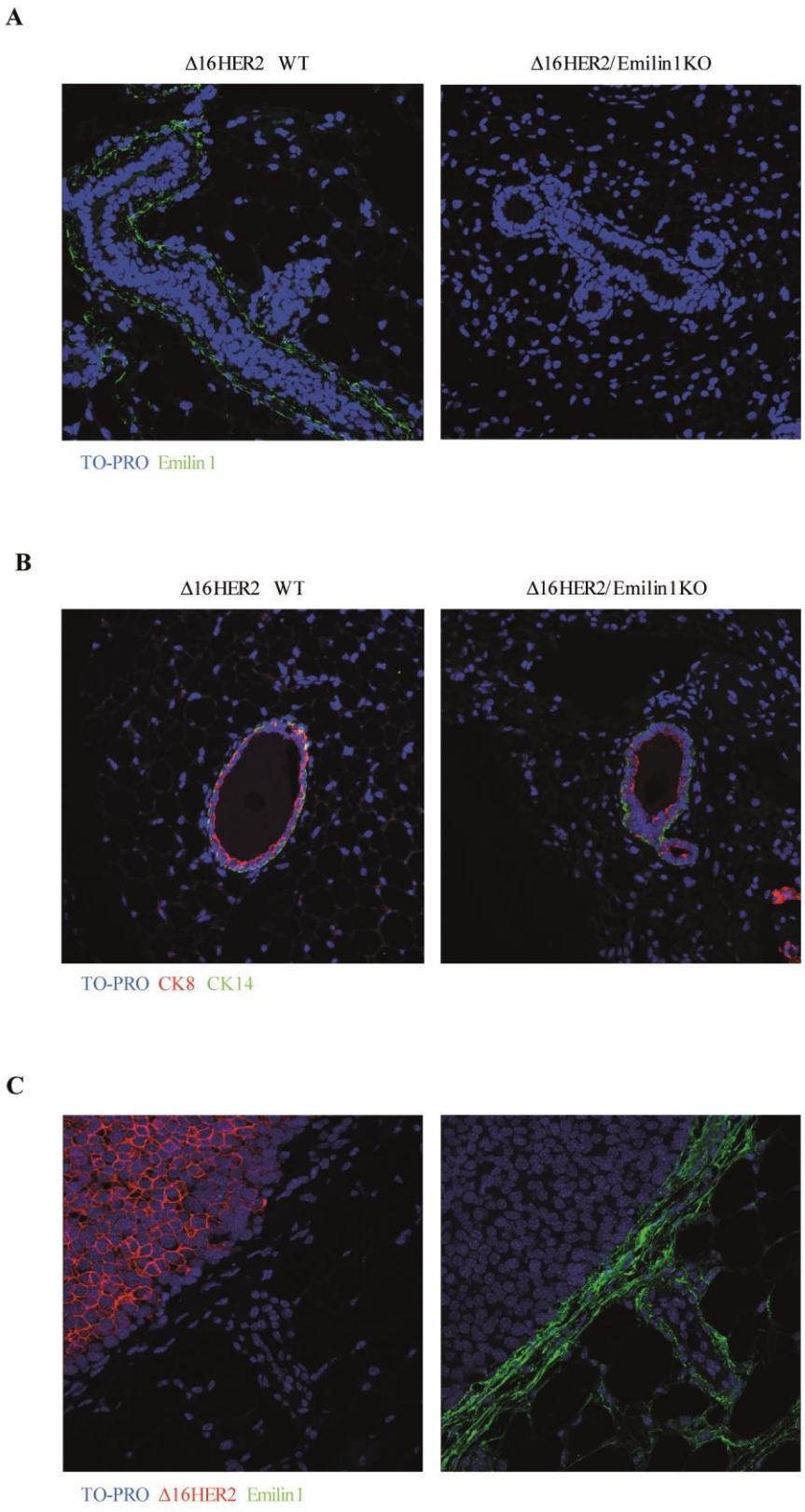

Figure 1. Emilin1 is localized in the extracellular matrix that surrounds the ductal tree of the mammary gland and the tumor mass. Its absence does not alter the localization of citokeratin 8 and 14. **A**, pictures depicting the deposition of Emilin1 in the mammary gland architecture of Δ16HER2 WT animals and its absence in the Δ16HER2/Emilin1KO mice. **B**, citokeratin 8 and 14 deposition in the mammary gland of Δ16HER2 WT and Δ16HER2/Emilin1KO mouse models. **C**, representative immunofluorescence of tumor mass stained for HER2 and Emilin1.

To deeper investigate the effects caused by the absence of Emilin1 in the context of Δ16HER2 driven tumorigenesis, we collected mammary glands from two cohorts of virgin females, from both genotypes (Emilin1 WT and KO). One cohort was sacrificed at 11 weeks (n. 5/genotype) and the other at 13 weeks of age (n. 5/genotype). The morphological analysis, conducted by whole mount staining, showed no differences at 13 weeks of age, also because there was a high variability observed within the same genotype, possibly due to the hormonal status of the moment in which MMG were collected (Figure 2A). On the contrary, looking at the mammary gland architecture at an earlier phase of development, at 11 weeks of age, we observed a robust difference between the two genotypes (Figure 2A). In fact, Δ16HER2/Emilin1KO mice showed a higher degree of side branching and an initial process of alveologenesis that was almost absent in Δ16HER2 WT mice, thus highlighting a different stage of mammary gland development between the two genotypes (Figure 2A). To better characterize these differences, we employed real-time PCR and western blot techniques, analyzing the main actors involved in the mammary gland development (Figure 2B and 2C). It is already known that estrogen, progesterone and prolactin hormones, whose levels are tightly regulated during MMG development, play fundamental roles in the different stages of branching and alveologenesis. Estrogen levels have been found to be higher during puberty, mainly regulating the ductal elongation and bifurcation. On the contrary, progesterone is more active during the side branching process and during the alveologenesis process, together with prolactin. Finally, prolactin is the main actor of the lactogenic differentiation. To look at the expression of these hormones in our cohorts of mice sacrificed at 11 weeks of age, we extracted the RNA and proteins from the MMG tissue and observed that Δ16HER2/Emilin1KO mice displayed a significantly higher expression of progesterone receptor (PR), both at RNA and protein level (Figure 2B and 2C), indicating an increased side branching process when compared with wild-type littermates. Given these results, we decided to look at all known regulators of the secondary branching during MMG development, such as prolactin receptor (Prl-R), Elf5, TGF-β2 and RANK-L (Zhou et al., 2005; Harris et al., 2006; Choi et al., 2009). The results from this analysis demonstrated the same trend for the RNA levels of all these target, confirming that there was a different transcriptional program governing MMG development between Emilin1 WT and KO mice. On the other hand, estrogen receptor (ER) that plays a key role in the process of elongation and primary branching, was higher in the WT mice, especially at the protein level (Figure 2B). This result suggested that while the ductal elongation/bifurcation stage was still ongoing at 11-weeks of age in female Δ16HER2/Emilin1WT animals, at the same age the KO counterpart was already going through a subsequent stage, in which estrogen has already carried out its function and it is now downregulated to allow the side branching driven from progesterone and prolactin (Figure 2B and 2C).

Finally, immunofluorescence analysis of the proliferation marker Ki-67 demonstrated a slightly increased proliferation in Δ16HER2/Emilin1KO MMG, at both 11 and 13 weeks of age, when compared with MMG of Δ16HER2/Emilin1WT mice (Figure 2D and 2E).

Together, these data indicated that Δ16HER2/Emilin1KO female mice display an acceleration in the developmental of the mammary gland.

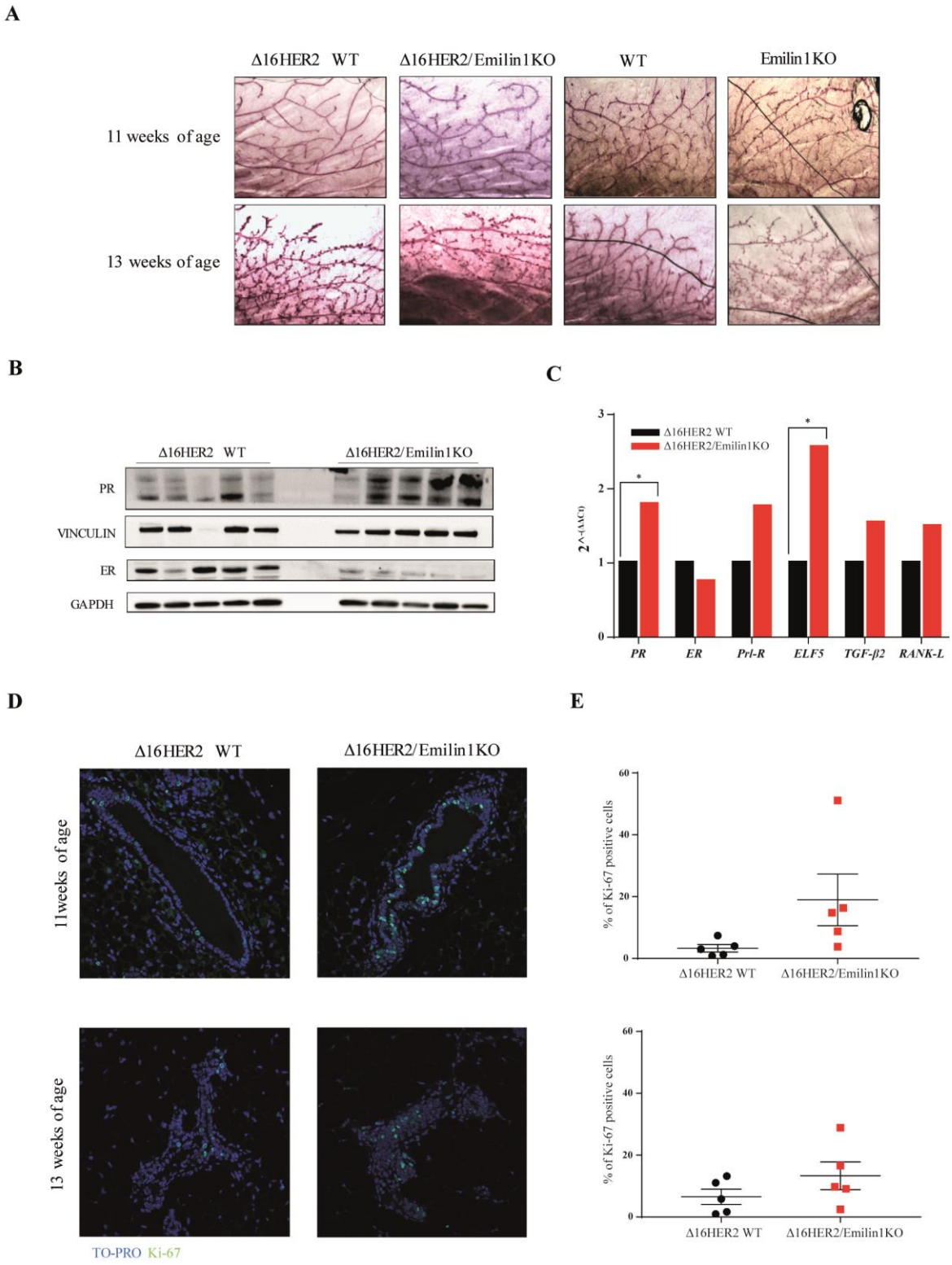

Figure 2. Emilin1 regulates mammary gland development and cell proliferation. **A**, whole mount staining depicting the increased side branching in the mammary gland of Δ16HER2/Emilin1KO mice at 11 weeks of age compared with the Δ16HER2 WT animals. No important differences were detected at 13 weeks of age. **B**, protein levels and (**C**) RNA expression of some key regulators of the mammary gland development in 11-weeks old mice. **D**, immunofluorescence representing the increased cell proliferation index displayed by the Emilin1-ablated mammary gland in 11 and 13-weeks old animals with (**E**) the relative percentage of Ki-67-positive cells. Five mice per genotype were evaluated.

3.2 Characterization of the Δ16HER2-driven mammary tumorigenesis in Emilin1KO mouse model

Given the results obtained in the context of normal MMG development, we asked whether this increased development and these hormonal alterations that we observed in Δ16HER2/Emilin1KO female mice could also impact in mammary tumorigenesis. We started the characterization of Δ16HER2/Emilin1WT and Δ16HER2/Emilin1KO mice evaluating the onset of palpable tumors and then measuring the tumor growth. Loss of Emilin1 led to a remarkable anticipated onset of palpable tumors compared to the WT counterpart (13.32 *vs* 15.28 weeks) (Figure 3A). Then, we followed tumor growth over time, by measuring tumors once a week, over a period of 11 weeks after the initial onset. However, no significant difference was observed between the two cohorts (Figure 3B).

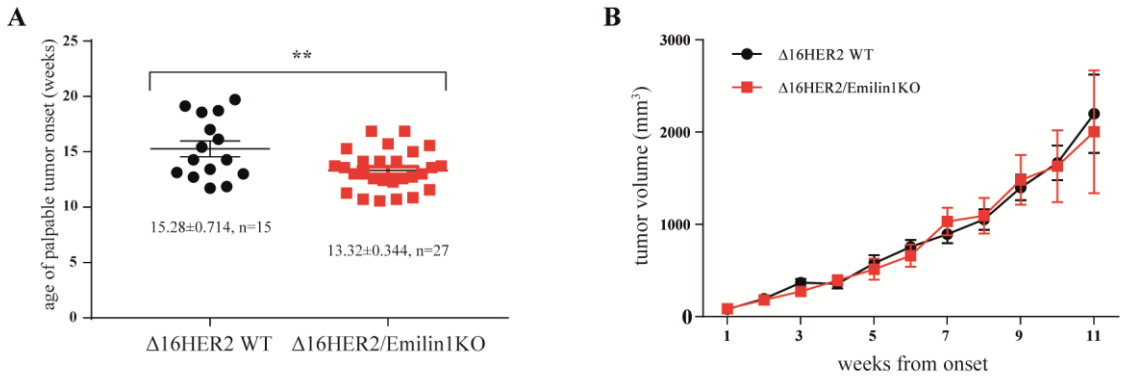

Figure 3. Emilin1 loss induces an impairment of the tumor onset, but it does not affect the tumor growth rate in Δ16HER2-driven tumorigenesis. **A** and **B**, graphs report the onset (**A**) and the growth (**B**) of palpable tumors derived from Δ16HER2 WT (15.28 weeks) and Δ16HER2/Emilin1KO (13.32 weeks) female mice. The animals were monitored twice a week, and tumors were followed up and measured for 11 weeks after tumor appearance.

To deeply investigate the involvement of Emilin1 during tumor initiation and study the early steps of tumorigenesis, we next collected mammary gland and, if present, tumor masses, in cohorts of mice sacrificed at 13 weeks of age, the time point at which we could observe the formation of first palpable tumors in Δ16HER2/Emilin1KO mice. These MMG were employed to evaluate the number and size of tumor foci, by Hematoxylin and Eosin (H&E) staining (Figure 4A). Data collected from the staining pointed out a slightly higher number of tumor foci in Δ16HER2/Emilin1KO mice, which possessed also larger areas compared to the WT counterpart (Figure 4B and 4C).

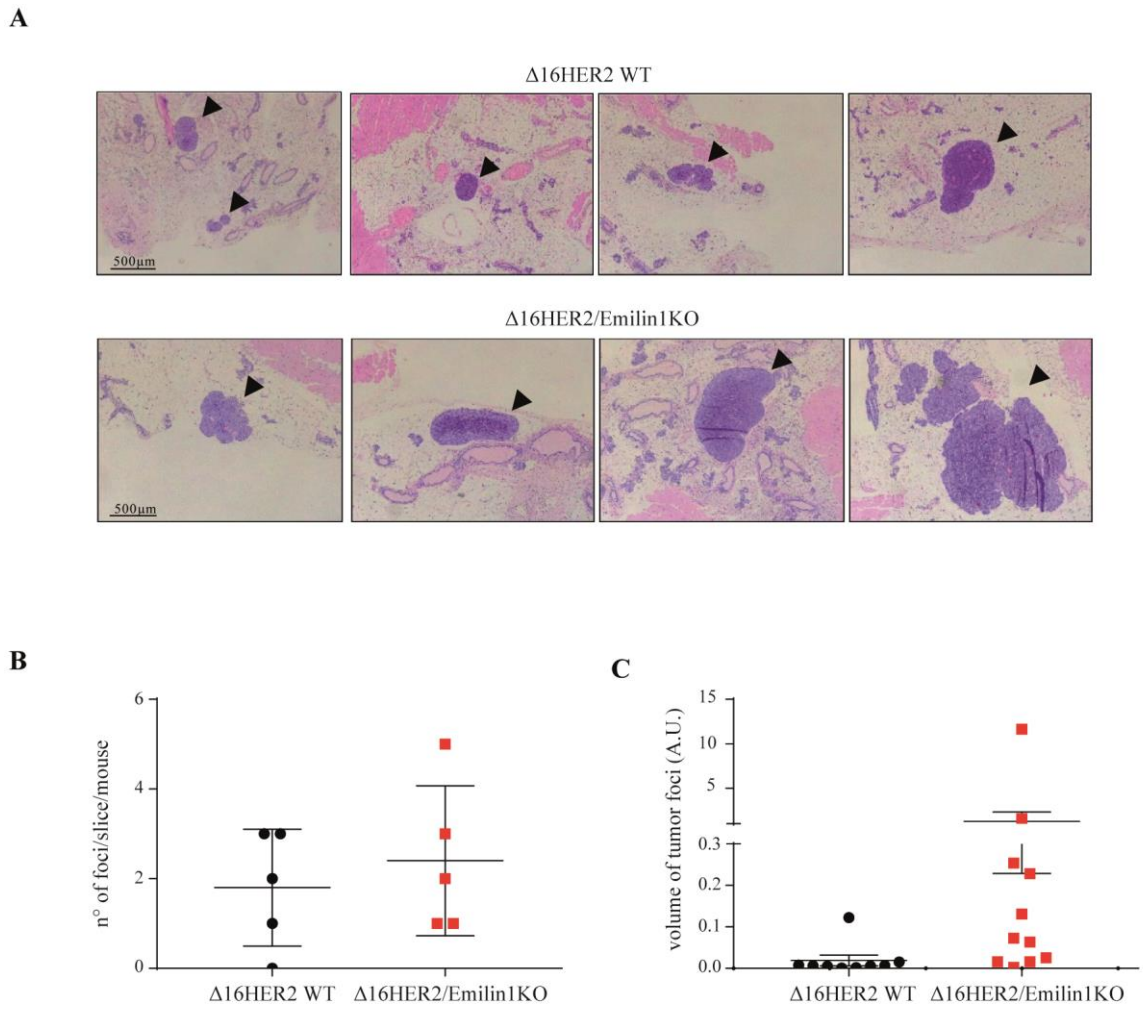

Figure 4. Δ16HER2/EmilinKO mice present increased tumor dimensions and a significant increase in tumor number. **A**, representative images of hematoxylin and eosin–stained mammary glands. Tumor foci are indicated by black arrows. Graphs report (**B**) the number of neoplastic foci detected per hematoxylin and eosin–stained section of mammary glands collected from Δ16HER2 WT or Δ16HER2/EmilinKO mice at 13 weeks of age and (**C**) their volumes. Both the third and the fourth mammary gland were evaluated and at least n = 5 mice/genotype were scored.

We then repeated the same experiment, but using cohorts of mice sacrificed at 11 weeks of age. In these MMG, H&E staining was not sensitive enough to detect the very small tumor foci that could be present at this early stage of tumor initiation (not shown). We thus decided to employ immunofluorescence techniques and western blot analysis, to better investigate the presence of small tumor foci based on Δ16HER2 positivity, which could be easily assessed by WB and IF even if present at single (or few) cell level. The western blot pointed out that higher levels of Δ16HER2 protein were present in the MMG of 11 weeks-old female Δ16HER2/Emilin1KO mice (Figure 5A).

Accordingly, the immunofluorescence analysis confirmed the presence of a significantly higher number of tumor foci that were also bigger in size, in Δ16HER2/Emilin1KO cohort compared to the Δ16HER2/Emilin1WT one (Figure 5B, 5C and 5D).

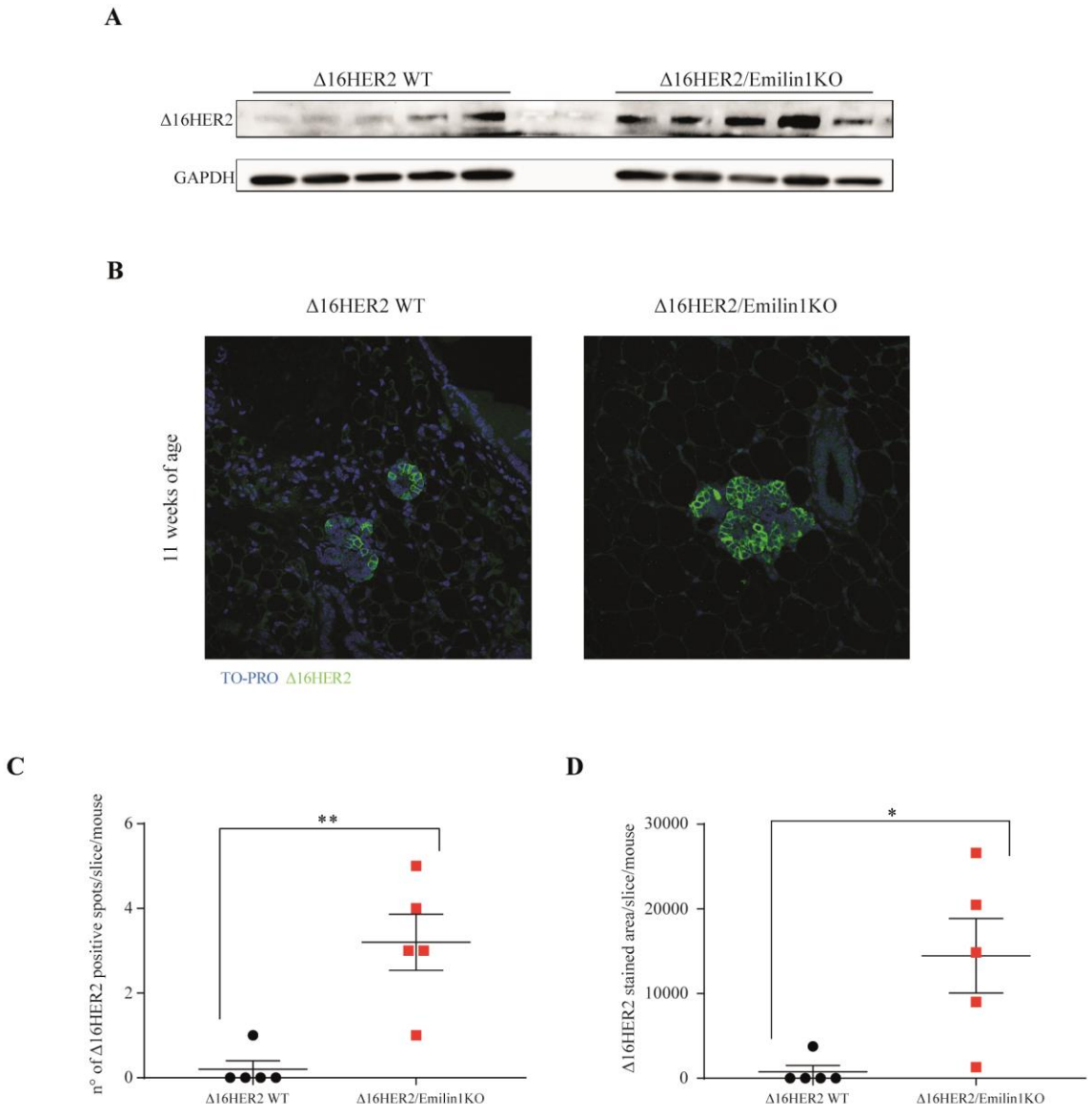

Figure 5. Δ16HER2/EmilinKO mice exhibit a higher number of tumor foci and an increased tumor volume. **A**, western blot reporting the protein level of Δ16HER2 in Δ16HER2 WT and Δ16HER2/Emilin1KO mice at 11 weeks of age. **B**, representative immunofluorescence depicting the dimension of tumor foci in the two genotypes. Graph representing (**C**) the number of tumor foci/slide/mouse and (**D**) their dimension.
At least n=5 mice/genotype were analyzed in each experiments.

Together, these data supported the notion that loss of Emilin1 provided an advantage for initiation of Δ16HER2-driven mammary tumorigenesis.

3.3 Mammary adipose tissue morphology in Δ16HER2/Emilin1KO mice

Among the risk factor for different types of cancer, obesity represents one of the top listed one, particularly in BC (Brown et al., 2021). Literature data report that the risk of BC increases by 10% for every BMI unit above 25 (Lauby-Secretan et al., 2016). This risk arises from the fact that obesity-related factors regulate many signaling pathway that are strictly linked to cancer, such as phosphoinositide 3-kinase (PI3K)–RAC serine/threonine-protein kinase (AKT), hypoxia-inducible factor 1α (HIF1α), liver kinase B1 (LKB1)–AMP-activated protein kinase (AMPK) and p53 (Brown et al., 2021). From a macroscopic observation of the mice and from the dissection of the MMG carried out for the initial characterization described above, we repeatedly observed that Δ16HER2/Emilin1KO mice were bigger and displayed a higher amount of fat in the MMG. To assess the validity of these observations, we decided to follow the growth in weight of the two genotypes, with or without Δ16HER2, from week 4 to week 13 of their life. However, from this analysis we could not highlight any significant difference (data not shown). Next, we looked at the adipose tissue present in the MMG, by looking at the H&E staining of the cohorts of mice shown in Figure 6A. We acquired three different fields for each sample, evaluating both the third and the fourth mammary gland for each mouse (n. 5/genotype). The analysis was conducted measuring the area of the adipocytes and calculating the average area, in the two mammary glands of each mouse (Figure 6B). From this analysis we observed that Δ16HER2/Emilin1KO displayed a slightly higher adipocytes dimensions, which might be in line with the anticipated tumor onset that we observed. To better investigate this phenotype, we then looked at the lipid metabolism, to verify whether this increased mammary gland adipose tissue was connected to an overall augmented fatty acid synthesis. Using quantitative real-time PCR (qRT-PCR), we thus evaluated several key actors of the lipid metabolism. However, our data showed that indeed, most of them were expressed at lower level in the MMG from Δ16HER2/Emilin1KO mice (Figure 6C). It is important to note that an increased fatty acid synthesis does not always relate to obesity. The extracellular bioavailability of different fatty acids is an important variable that can impinge on *de novo* lipid synthesis (Röhrig et al., 2016) and indeed lipid deprivation may increase the activity of different enzymes involved in the fatty acid synthesis (Ferraro et al., 2021). This scenario may suggest that the fatty acids synthesis in the Δ16HER2/Emilin1KO mice could be less active due to a higher extracellular bioavailability of lipids. This hypothesis will

need further studies to be confirmed and it is certainly an intriguing possibility that we intend to pursue in our future experiments.

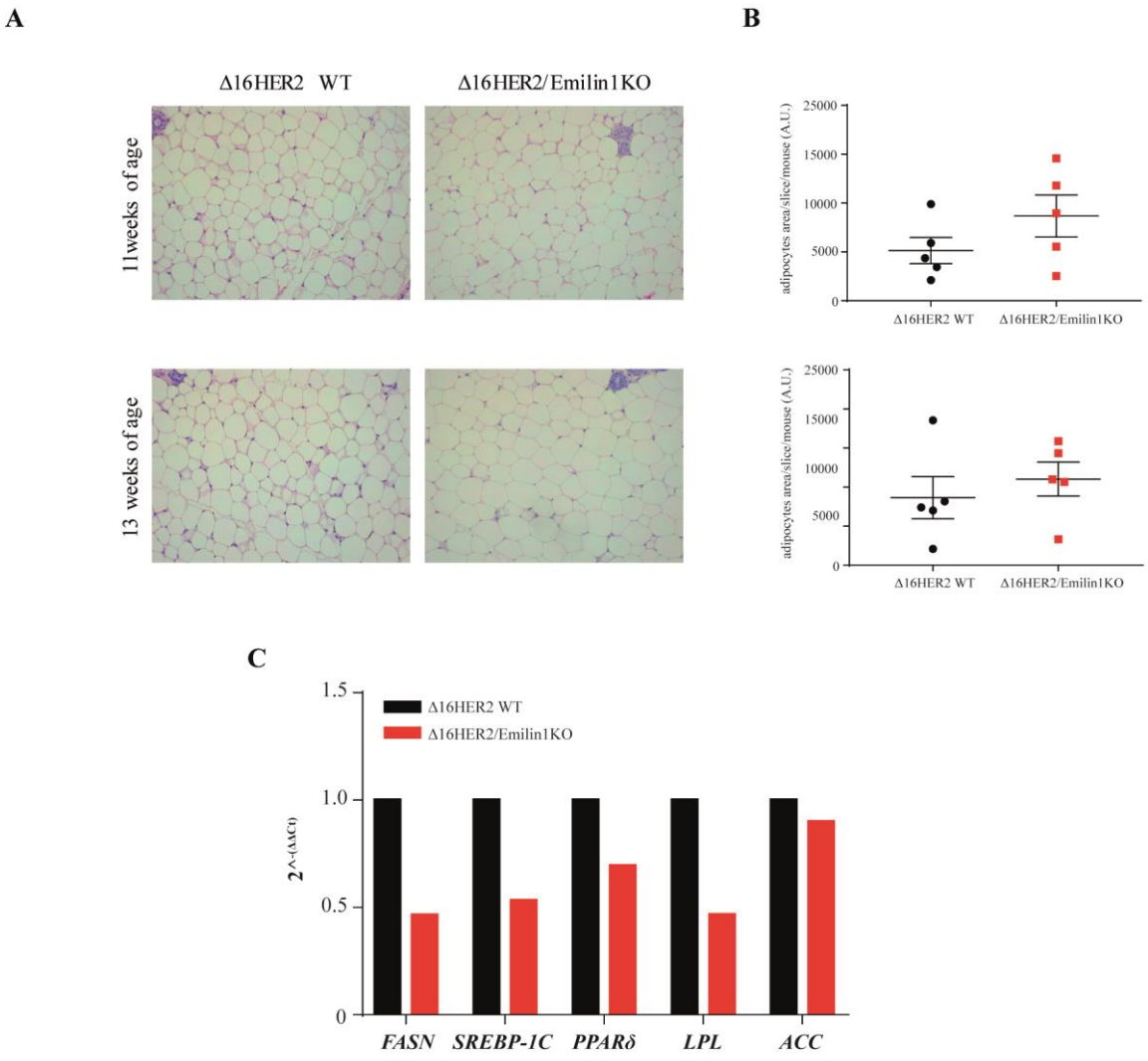

Figure 6. Emilin1 deficiency enhances adipocyte dimensions in the mammary gland. **A**, hematoxylin and eosin staining of mouse mammary fatpad. Pictures were taken looking at the area with the biggest adipocytes in each slide. Both the third and the fourth mammary gland were evaluated and at least 3 fields for each slide were analyzed. 20X magnification. **B**, graphs representing adipocyte dimensions for each mouse. **C**, qPCR gene expression analysis of key regulators of the fatty acid synthesis.

3.4 Evaluation of the elastic fiber deposition in the mammary gland

Stiffness of the matrix, in which cells are immersed, is a widely known factor that influences cell behavior, in both healthy tissues and cancer (Wells et al., 2008; Chaudhurie et al., 2014). An increased stiffness strongly impinges on tumor development, tumor cells proliferation, angiogenesis,

metastases, resistance to chemotherapy, and genetic instability (Kalli et al., 2018; Huang et al., 2021). Emilin1 deposition has been described to be quite peculiar, since this ECM protein is present in several tissues in association with elastic fibers, especially at the interface between the fibrillin microfibrillar scaffold and the elastin core (Bressan et al., 1993). Further studies also highlighted the interaction of Emilin1 with some components of the elastic fibers (Schiavinato et al., 2016; Schiavinato et al., 2017). Thus, we decided to investigate the deposition of elastic fibers in the mammary tissue of 11-weeks old mice, to understand whether Emilin1 loss impacted on this aspect and whether the anticipated onset displayed by Δ16HER2/Emilin1KO might be ascribed, at least in part, to an altered stiffness of the extracellular matrix. To shed light on this point, we employed the Masson's trichrome staining, which is a three-color staining widely used to evaluate the deposition of the elastic fibers (especially collagens). Briefly, by staining with Masson's trichrome it is possible to highlight keratins and muscle fibers in red, collagen or bone in blue, cellular cytoplasm in pink and nuclei in dark brown. We stained one slice per mammary gland, including both the third and the fourth MMG for each mouse (n. 5/genotype) (Figure 7A). At least five ducts per mammary gland were analyzed. The evaluation of the amount of elastic fibers was performed calculating the ratio between the area covered by the collagens (blue staining) around the mammary ducts and the total area of the ducts for each mammary gland. Then, we calculated the average between the two mammary glands evaluated and compared the two genotypes. However, by this analysis we did not highlight strong differences between the two genotypes (Figure 7B).

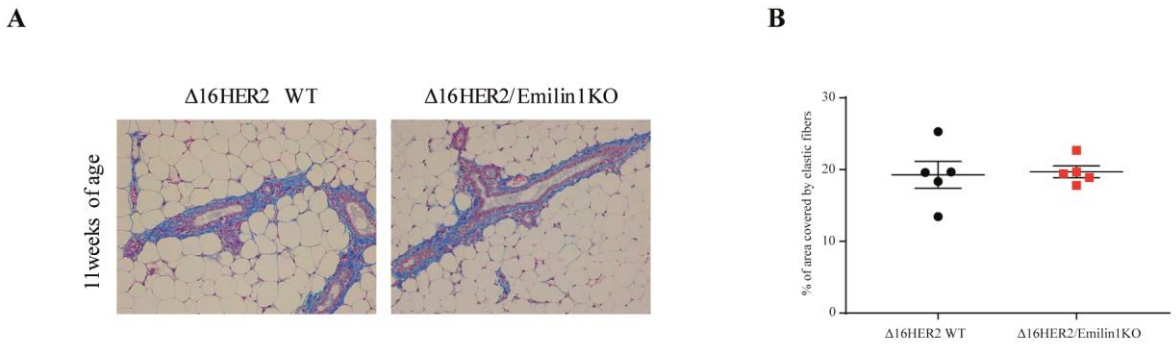

Figure 7. Emilin1 absence does not alter the deposition of elastic fibers in the mammary gland. **A**, Masson's trichrome staining of mouse mammary gland. Both the third and the fourth mammary gland were evaluated and at least 5 fields for each slide were analyzed. 20X magnification. **B**, graphs representing the percentage of the area covered by elastic fibers (blue dye) respect to the total area of the duct.

This evaluation of the stiffness of the matrix was very approximate and preliminary, since it is known that the amount of collagens strongly influences the rigidity of the matrix (Tang et al., 2020). Further experiments will be carried out to rule out the role of Emilin1 in stiffness of mammary gland ECM.

3.5 Lymph nodal spreading in Δ16HER2/Emilin1KO mice

The axillary lymph nodes status is a very important prognostic factor for patients affected by primary BC (Jatoi et al., 1999; Klauber et al., 2006). Literature data and previous studies from our lab demonstrated that Emilin1 KO mice are affected by structural and functional defects of the lymphatic system, displaying mild lymphedema, a significant drop in lymph drainage and an enhanced leakage of lymphatic vessels (Danussi et al., 2008). Moreover, in a two-stage model of skin carcinogenesis, the ablation of Emilin1 in CD1 and C57BL/6 mice enhanced the lymphangiogenic process, both in the tumor and in the lymph nodes closer to the tumor mass (Danussi et al., 2012). In accordance to this result, also the tumor growth and the lymph node metastasis were higher in Emilin1 KO mice, altogether suggesting a protective role of Emilin1 in metastatic spreading through the lymphatic circulation (Danussi et al., 2012). In light of these important considerations, we decided to look at the pattern of lymph nodal metastases of our Δ16HER2 mice. As a first approach, we sacrificed mice after 13 weeks from the tumor onset, in cohorts of FVB Δ16HER2/Emilin1WT and Δ16HER2/Emilin1KO mice (n. 3/genotype). This time point was chosen as late as possible to have primary tumor masses in an advanced stage, but early enough to avoid suffering of the animals. We thus collected the axillary lymph nodes from mice, after highlighting their presence by Evan's blue staining. Lymph nodes were then fixed in formalin, cut and immunostained for Δ16HER2. However, the immunofluorescence staining did not identify the presence of any HER2+ cancer cells in any of the lymph nodes collected, indicating that lymphnodal metastatic spreading was not present in this model, at least at this time point (data not shown). Given the high aggressiveness of the Δ16HER2, it was not possible to conceive a later time point for metastatic evaluation of these FVB mice. We thus decided to change model and background, moving to C57BL/6 Emilin1 KO mice syngenically injected with EO771E2 BC cells, which express HER2 (Wang et al., 2014). In a pilot experiment, mice (n. 3/genotype) were bilaterally injected with EO771E2 cells in the third MMG and then sacrificed at different time points. One mouse for each genotype was sacrificed when the tumor masses reached critical dimensions, while the others were subjected to surgical resection of the tumor masses and let alive for a longer period. After approximately 1 weeks from surgery, local recurrences arose in the MMGs and, when these recurrences reached again critical dimensions, mice were sacrificed (Figure 8A). Lymph nodes were collected and subjected to the staining for Δ16HER2, as

described below. The immunofluorescence staining, although less clear in this organ compared to what we usually obtain in MMG and mammary tumors, demonstrated that there was some HER2 positivity in the lymph nodes of both genotypes (Figure 8B). However, given the very low number of mice employed and the need to optimize the staining in lymph nodal tissue, we cannot draw any conclusion so far and will need repeat this experiment in the future.

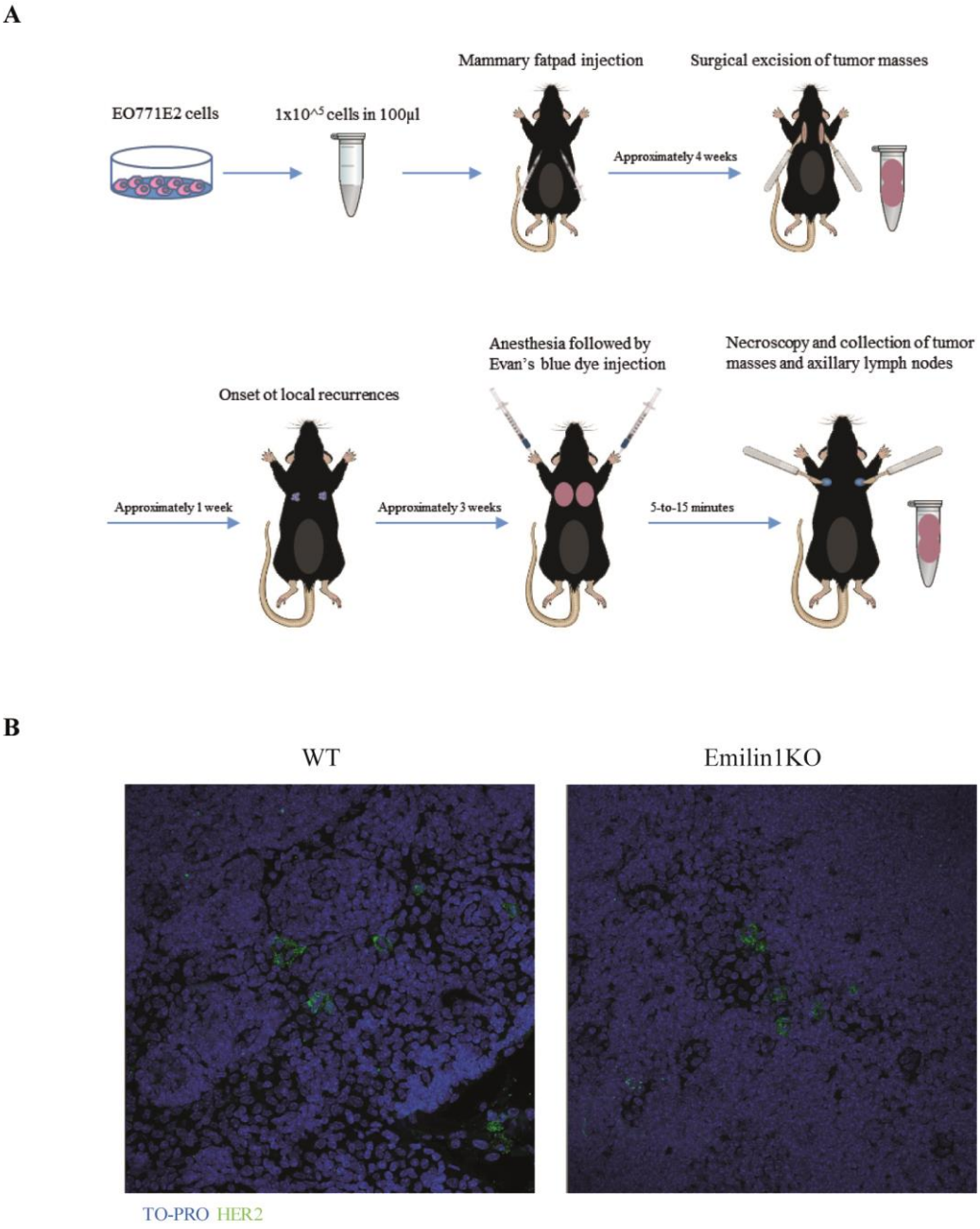

Figure 8. A, scheme representing the pilot experiment performed to to evaluate the metastatic dissemination of breast cancer cells through the lymphatic circulation . **B**, axillary lymph nodes pictures of C57BL/6 mice injected with EO771E2 showing the presence of positive cell for the HER2 staining.

3.6 Generation and characterization of the FVB MMTV-Δ16HER2/Emilin1-E933A mouse model

Literature data describe different functions of the Emilin1 domains, in particular regarding the N-terminal EMI domain and the C-terminal gC1q domain. The EMI domain is known for its ability to bind pro-TGF-β1, thus inhibiting its processing by furin convertases and preventing the maturation of the cytokine. In fact, it has been reported that Emilin1KO mice display higher TGF-β1 protein levels in different organs (Zacchigna et al. 2006; Capuano et al. 2019). On the other hand, the gC1q domain is required for Emilin1 trimerization and it is involved in the interaction with α4β1 and α9β1 integrins. Through this interaction, Emilin1 controls skin homeostasis, carcinogenesis, and it also maintains the correct structure and function of the lymphatic vasculature. The anticipated tumor onset observed in Δ16HER2/Emilin1KO animals made us wonder whether the phenotype was caused by the absence of EMI domain, the gC1q domain or by the combined loss of both. To investigate this aspect, we took advantage of the Emilin1-E933A transgenic murine model that was generated and characterized in our laboratory. The E1-E933A mouse model express a human Emilin1 carrying the E933A mutation, which abolishes the ability to engage α4β1 and α9β1 integrins. This model was already tested for the expression of Emilin1 mRNA, which levels are very close to the wild-type ones (Capuano et al. 2019). In the same work, also TGF-β1 protein levels were evaluated, showing comparable levels with the wild-type counterpart. Starting from these notions, we crossed the E1-E933A mice with the Δ16HER2/Emilin1KO ones, to generate the Δ16HER2/Emilin1KO/E1-E933A (Δ16HER2/Emilin1KOtg) model. First, this new mouse colony was evaluated for the onset of palpable tumor, to investigate whether the EMI domain or the gC1q domain might be responsible of the anticipated tumor onset. Briefly, as reported above for the Δ16HER2/Emilin1KO animals, the tumor onset was assessed by palpation of the mice twice a week until the appearance of the first tumor mass was observed. By this analysis, we could establish that the Δ16HER2/Emilin1KOtg mice displayed a comparable onset with the Δ16HER2/Emilin1KO animals (13.27 vs 13.32 weeks) (Figure 17A). This result clearly indicated the importance of the gC1q domain and, thus, the binding to integrins, in regulating the tumor onset.

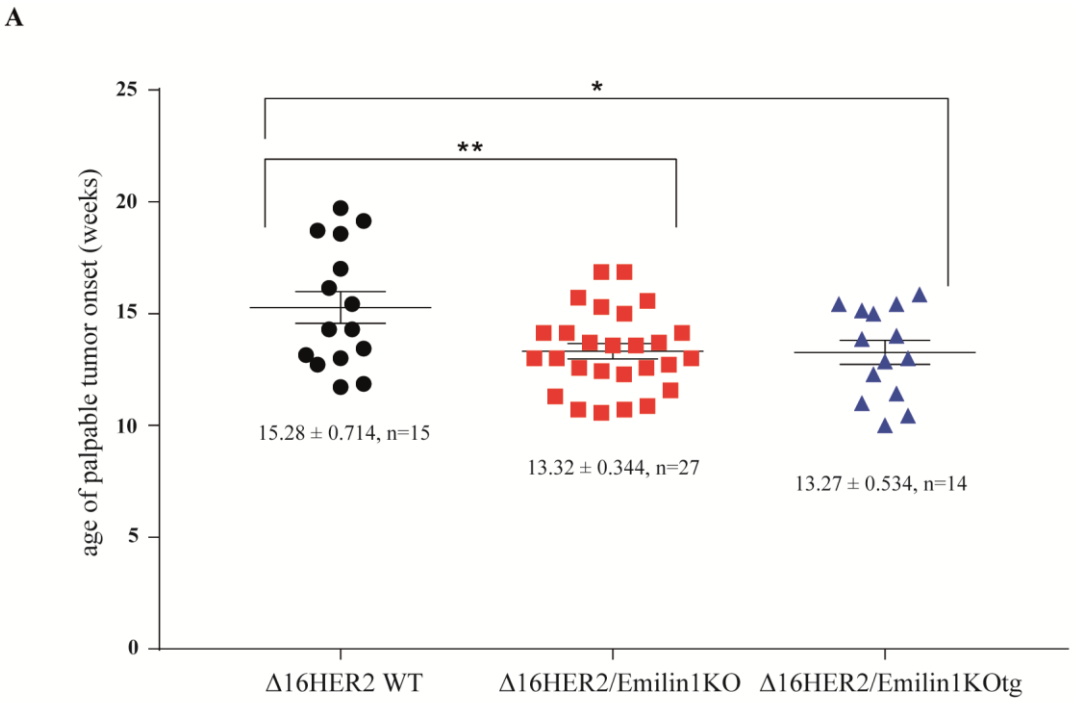

Figure 9. The Δ16HER2/Emilin1KOtg model displays anticipated tumor onset. **B**, Δ16HER2/Emilin1KOtg mouse present an earlier tumor onset respect to the Δ16HER2 WT mouse, and it is comparable to the one of the Δ16HER2/Emilin1KO mice.

Altogether, these results point out a role for Emilin1 in the regulation of mammary gland architecture. Emilin1 seems to accelerate mammary gland development through the regulation of key hormonal players in this process and to increase the adipocyte dimensions in the mammary tissue. Moreover, the results collected from the Δ16HER2-driven BC model clearly indicated that Emilin1 played a suppressive role in tumor initiation, while is did not affect tumor growth. These results might be partially explained by the deposition of Emilin1, which is present only in the extracellular matrix surrounding the tumor mass, but not inside. Thus, as the tumor grows Emilin1 loses contact, and possibly control, with most of BC cells. The role of Emilin1 in BC nodal metastases still need further investigation and future experiments will clarify if loss of Emilin1 may impact on this critical aspect of BC progression.

4. DISCUSSION

4. DISCUSSION

The mammary gland is a perfect example of a dynamic and plastic tissue able to perform dramatic changes during its developmental process, with cells that simultaneously receive and react to several stimuli, eventually leading to proliferation, differentiation or apoptosis. In a close way, the mammary gland reacts to stimuli induced by aberrantly activated pathways, during breast tumorigenesis (Visvader, 2009; Inman et al., 2015). The extracellular matrix plays a key role in the maintenance of mammary gland structure, and it is a well-known supplier of external signals and stimuli that regulate the mammary gland plasticity. Because of its fundamental importance, alterations of the ECM might be reflected in alterations of the mammary gland structure, that may be implicated in different steps of breast tumorigenesis. Emilin1, a protein of the ECM that was found to be closely associated with elastic fibers, is known to be involved in the maintenance of skin homeostasis and in the regulation of skin carcinogenesis, where it impinges on tumor cell proliferation and lymph node invasion. Moreover, Emilin1 knockout (KO) mice display increased cell proliferation and enhanced lymphangiogenesis both in skin papillomas and sentinel lymph nodes (Danussi et al., 2012). These data suggest a protective role of Emilin1 in tumor growth, in lymphatic vessel formation and metastatic spread to lymph nodes. The role of Emilin1 in the mammary gland and in BC tumorigenesis has still to be elucidated. From literature, it is known that Emilin1 mRNA level changes based on BC grade, decreasing in grade II tumors and slightly increasing in advanced grade III cancers. Protein levels measured by western blot technique show increased levels of Emilin1 in grade I tumors when compared with control, with a strong decrease in grade II BC (Rabajdova et al., 2016). Among the BC classification, the HER2-enriched subtype takes into account for 15-25% of all BC and they are often diagnosed as high-grade tumors. One of the naturally occurring splicing variant of the HER2 receptor is the Δ16HER2 variant, which is characterized by the skipping of exon 16 that impairs the intramolecular disulphide-bridges. As a consequence, the remaining cysteine residues are able to form intermolecular bonds, leading to homodimerization and constitutive activation of the receptor. We employed the FVB-MMTV Δ16HER2 murine model to better characterize the Emilin1 role in the mammary gland and in BC. First of all, we intercrossed FVB-MMTV Δ16HER2 males with the Emilin1 KO female mice that were already present in our animal facility. Once the new murine model was generated, we proceeded with a first evaluation of the mammary gland structure by whole mount staining, discovering that ablation of Emilin1 impacted in the mammary gland architecture, accelerating its development. We observed that Δ16HER2/EmilinKO mice are already undergoing the secondary branching process and an initial alveologenesis at 11 weeks-of-age, while the wild-type counterpart was still carrying out the ductal elongation/primary branching step. This observation was also supported by western blot and qRT-PCR data, which showed that mammary

glands from Δ16HER2/EmilinKO female mice displayed higher levels of progesterone receptor and prolactin receptor in comparison with their WT littermates. Progesterone receptor has a well-known role in leading the secondary branching of the mammary gland, while prolactin receptor is mainly involved in the aveologenesis process. Moreover, the Emilin1 KO mammary gland displayed a slightly increased proliferation index, both at 11 and 13 weeks of age, suggesting that Emilin1 might exerts an anti-proliferative effect within the mammary gland microenvironment. This observation was in line with previous studies that highlighted the role of Emilin1 in regulating cell proliferation in the skin compartment. This anti-proliferative role can also impinge in breast tumorigenesis, accelerating tumor foci appearance and increasing tumor growth rates in the Emilin1KO context. Looking at the onset of palpable tumors, we observed that Δ16HER2/Emilin1KO mice exhibited an anticipated tumor onset. However, quite unexpectedly, the tumor growth rates were indistinguishable between genotypes. These data may suggest that Emilin1 plays a tumor suppressor role in breast tumorigenesis, but this role could be of relevance only in the first steps of the process. We can speculate that, at this early stage, the activation of the very aggressive Δ16HER2 oncogene is probably not widespread enough to overcome the protective role of Emilin1, while it takes over in the later stages and no difference in the tumor behavior is then observable looking at the two genotypes. We also demonstrated that Emilin1 is localized in the extracellular matrix that surrounds normal mammary ducts and the tumor mass, whereas it is completely absent inside the tumors. This peculiar localization of Emilin1 might allow to impact only in the first stages of BC tumorigenesis, when the tumor foci are still at the beginning and the extracellular matrix stimuli are yet able to impact on the oncogene behavior. To better characterize the anticipated tumor onset of Δ16HER2/Emilin1KO mice, we decided to analyze mice at 13 weeks of age, that is a useful time point to detect the presence of the initial tumor foci, since tumor masses are still too small to be detected by palpation. The observation of tumor foci has been carried out by hematoxylin and eosin staining, a classic histological staining. Tumor foci have been detected looking for abnormal aggregates of epithelial multinucleated cells, which often display aberrant mitosis and irregular edges. At this stage, Δ16HER2/Emilin1KO mice displayed a slight increase of tumor foci number per slice/gland/mice, which were also bigger in size when compared with the wild-type counterpart. These data perfectly match with the anticipated onset of palpable tumors observed before. We thus decided to analyze also 11 weeks old mice, to better confirm these differences. Tumor foci were still too small to be detected by hematoxylin and eosin at this stage, so we employed immunofluorescence staining and western blot analysis to describe in a more accurate way the differences between the two genotypes. We stained the 11 weeks of age mammary gland slices with an anti-HER2 antibody, which allowed an easy observation of the small tumor foci already present in the gland. Tumor foci displayed

by the Δ16HER2/Emilin1KO mice were significantly higher in number and in dimension compared to the wild-type littermates. Moreover, we further confirmed these differences by western blot analysis, detecting a higher level of HER2 protein in the KO mice. All these data strongly agree with the macroscopic analysis of tumor appearance carried out before, and point out a possible tumor suppressor role of Emilin1 in the mammary gland microenvironment, at least in the first steps of tumorigenesis. Mammary gland analysis of Δ16HER2/Emilin1KO mice also pointed out the bigger dimensions of the adipocytes in the tissue. Since obesity is a strong risk factor for BC development, further studies might be of great interest to evaluate the connection with the anticipated tumor onset displayed by our model. Further investigation of the adipocyte phenotype might be of particular interest in the context of obesity-related BC since it impinges in the initiation of tumorigenesis and it is a controllable risk factor for this type of cancer. Another possible explanation for the differences we observed in the tumor initiation could be ascribed to a different matrix stiffness caused by the ablation of Emilin1. However, our preliminary evaluation based on the content of the elastic fibers in the mammary gland did not display evident abnormalities, but additional studies are needed to better assess this point. Furthermore, due to the importance of lymph node metastases in BC and because of the proven role of Emilin1 in the maintenance of lymphatic homeostasis and in the regulation of lymphnodal metastases in other cancer types, we tried to evaluate the spreading of BC cells to the axillary lymph nodes. However, our first approach using the FVB MMTV-Δ16HER2 mice failed, due to the complete absence of nodal metastases in this model. On the contrary, our pilot experiment performed with C57BL/6 mice injected with EO771E2 cells demonstrated that this approach is feasible and will therefore further investigated in the future. In fact, some positive cells for HER2 immunostaining have been found in the axillary lymph nodes, even if their nature and the possible difference induced by loss of Emilin1 will need additional studies. A better understanding the possible role of Emilin1 in nodal metastases is fundamental since it is the preferential homing site for BC cells and it a strong prognostic factor in BC recurrence. Finally, we wondered about which Emilin1 domain could be responsible for the observed phenotype. The most likely candidates were the N-terminal EMI domain, able to tightly regulate TGF-β maturation and consequently the blood pressure homeostasis, and the C-terminal gC1q domain, responsible for the interaction with the α4β1 and α9β1 integrins. The Emilin1KO-E1-E933A mice helped us to shed light on this question. This model was previously generated in our lab and deeply characterized, ensuring comparable mRNA and protein levels of Emilin1 with the WT counterpart in different tissues and the intact function of the EMI domain. This model is basically an Emilin1KO mouse model in which the mutated gene of human Emilin1 has been inserted. The E933A mutation critically impairs the interaction between the C-terminal gC1q domain of Emilin1 and the α4β1 and α9β1 integrins, abolishing the anti-proliferative

action of Emilin1. First of all, we intercrossed Δ16HER2 males with Emilin1KO-E1-E933A females and generated a new mouse colony that we named Δ16HER2/Emilin1KOtg. Then, we evaluated the onset of palpable tumors and compared the results with the Δ16HER2 WT and Δ16HER2/Emilin1KO mice data. Interestingly, the median age of mice at palpable tumor onset was strongly in line with Δ16HER2/Emilin1KO data, thus suggesting that the main actor in modulating this phenotype was the C-terminal gC1q domain of Emilin1, the one missing in this mutant and responsible for the interaction with integrins.

Altogether, these data suggest that Emilin1 has a role in controlling mammary gland development and BC initiation, in a murine model of HER2+ BC. The precise mechanism behind the tumor initiation phenotype has still to be fully elucidated, but our data suggest that it might related to the interaction between the gC1q domain of Emilin1 and the α4/α9β1 integrins. Investigating this phenotype will be very important since integrins stimulate EGFR signaling through increased EGF secretion and HER2 clustering in BC cells, thus resulting in increased proliferation and, also, in trastuzumab resistance (Wang et al., 2009). Moreover, α4β1 integrin, which is a known interactor of Emilin1, is involved in the homing of endothelial and monocyte precursors to tumors (Jin et al., 2006), in the adherence of bone marrow-deriving cells to the tumor-associated endothelium and in the blood vessels density (Jin et al., 2006; Jin et al., 2006).

5. MATERIALS AND METHODS

5. MATERIALS AND METHODS

5.1 Animal experimentation

The Italian Ministry of Health and our Institutional Animal Care and use Committee (OPBA) approved the animal experimentation (authorizations #616/2015-PR and #630/2020-PR). All the in vivo experiments were conducted under the rigid regulation of OPBA and internationally accepted Institutional Animal Care and Use Committee guidelines for animal research and following the 3D principles. Mice colonies were housed in the animal facility of CRO Aviano under controlled environmental parameters (22°C with 40-60% of humidity), pathogen free condition and following a 12-hours dark/light cycle. All mice were monitored twice a week for the entire duration of the project and euthanized when required in agreement with the "AVMA guidelines on Euthanasia".

The MMTV-Δ16HER2 Emilin1 knock-out (E1ko) and the MMTV-Δ16HER2 Emilin1 knock-out/E933A (E1tg) mice were generated by intercrossing FVB male mice expressing the Δ16HER2 splicing variant (Marchini et al., 2011) with FVB female mice knock-out for Emilin1 and knock-out for Emilin1 carrying the E933A modified human Emilin1 protein respectively. All genotypes were verified by PCR analysis on DNA extracted from tail biopsies, using the MyTaq^{TM} Extract-PCR Kit (Bioline).

The sequence of primers used for the genotyping are listed below:

- Δ16HER2 Fw: 5'– GGTCTGGACGTGCCAGTGTGA – 3'
- Δ16HER2 Rv: 5' – GATAGAATGGCGCCGGGCCTT – 3'
- Emilin1 WT Fw: 5' – GAGGAGAGCGGAAGGAACTGAGG – 3'
- Emilin1 KO Fw: 5' – CGCCTTCTTGACGAGTTCTTCTGAG – 3'
- Emilin1 Rv: 5'– GAGGGAACAGAGCAGGAGGAGTG – 3'
- Emilin1 TG Fw: 5' – CACCTCGCAGGGCTGGCGGTG – 3'
- Emilin1 TG Rv: 5' – AGGAGCCCCAGGCCAGCTCTC – 3'

Agarose gel electrophoresis was used to detect PCR products. Gels were prepared using TBE-buffer 1X (Tris 54 Mm, EDTA 0.5 M pH8 20 mM, boric acid 27.5 mM) and added with Ethidium Bromide (Sigma-Aldrich).

5.2 Evaluation of tumor onset and progression in transgenic mice

Δ16HER2-bearing mice were monitored by palpation once per week to accurately determine the tumor onset from 8 weeks of age. Tumor progression was evaluated by caliper measurement and tumor mass volume was calculated with the following formula:

$$(Length \times Width^2)/2$$

Animals were euthanized at the endpoint of the experiment, at 11, 13 and 20 weeks of age, depending on the tumorigenesis stage examined. At the time of necroscopy tumor masses and mammary glands were collected for the analysis.

5.3 Collection of mouse mammary gland and whole mount staining

Thoracic and abdominal mammary glands were excised from the skin of virgin female mice at different weeks of age. Immediately after dissection, glands were spread on a glass slide and fixed in 4% paraformaldehyde (PFA) for two hours at room temperature (RT). Once fixed, PFA was eliminated by washing mammary glands in Phosphate Buffered Saline 1X (PBS, Sigma-Aldrich) and aqueous solution of 2% Carmine (Sigma-Aldrich) and 5% Alum (Sigma-Aldrich) was used to stain specifically the epithelial structures. Increasing concentrations of ethanol (EtOH) were then used to dehydrate the mounts (1 hour for each concentration). After that, mammary glands were immersed in xylol overnight (ON) at RT to delipidate the mammary fat pad and increase transparency. As last step, mammary glands were mounted with cover-slips using the Eukitt mounting media and analyzed under a stereo microscope (Leica M205 FA) at 10X and 20X magnification, as indicated.

5.4 Syngenic injection of EO771E2 cells and surgical excision of tumor masses

EO771E2 cells were maintained in DMEM medium (Gibco) supplemented with 10% of fetal bovine serum (Gibco) and 1% of penicillin/streptomycin (Sigma-Aldrich). $1x10^5$ cells were injected in the mammary fat pad of 8-weeks old females and the tumor growth was followed until the masses reached critical dimensions. At this point, one mouse per genotype was sacrificed and the axillary lymph

nodes were collected as described below. The tumor masses were also collected and stored at -80°C and in formalin. The tumors of the remaining mice were surgically resected and collected, and the recurrence was followed until the tumor masses reached again critical dimensions. The mice were then sacrificed and tumors and the axillary lymph nodes were collected.

5.5 Evan's blue staining and collection of axillary lymph nodes

Female mice were anesthetized and 2% Evan's blue dye was injected subcutaneously in the front footpad. After 10 to 15 minutes of anesthesia to allow the dye to travel through the lymphatic circulation, mice were sacrificed by cervical dislocation and dissected to localize the lymph nodes of interest. The blue-labeled axillary lymph nodes were collected in formalin and processed to obtain several slices at different levels.

5.6 Histological and immunofluorescence staining

Mouse thoracic and abdominal mammary glands explanted from 11 and 13 weeks of age where fixed in formalin ON, embedded in paraffin and cut into 2μm-thick sections with a microtome. Gland morphology and neoplastic foci presence were evaluated by Hematoxilin and Eosin (H&E) staining, and picture were taken under microscope at 5X and 10X magnification as indicated. At least 5 mice/stage/genotype were analyzed. Immunofluorescence (IF) staining were conducted rehydrating the specimens, immersing them in 10 mM citrate buffer pH 6.0 and performing the antigen retrieval by boiling in the microwave (550 W, 20 minutes). Samples were then left at RT until the cool down was complete. Permeabilization was performed with 0.2% Triton X-100 (Sigma Aldrich) in PBS for 5 minutes at RT for HER2 (Abcam). After permeab ilization step, the specimens were blocked in with 10% normal goat serum in PBS and then incubated ON at 4°C with the primary antibody. The incubation with secondary specific antibodies and TO-PRO-3 (Invitrogen) was performed the day after. For Ki-67 (Abcam) staining, samples were incubated at RT for 10 minutes with 0.4% Triton X-100 in PBS. After this passage, specimens were blocked with 10% normal goat serum in PBS and incubated ON at RT with the primary antibody. Incubation with secondary antibodies was performed as previously described. Primary antibody used were: HER2 (Abcam, #ab134182), Ki67 (Abcam, #ab15580) and Emilin1 (home-made). Second antibody used to perform the experiments were: (AlexaFluor® 488- or 568- -conjugated Invitrogen, 1:200). Specimens were analyzed with Leica SP8 confocal laser-scanning microscope connected with a Leica fluorescent microscope. LAS (Leica) and VolocityR (PerkinElmer) software were used to analyze the collected images. For Masson's

trichrome staining, mammary gland slices were dewaxed in deionized water and stained with hematoxylin for 5 minutes. The samples were then washed with tap water for 5 minutes and then briefly cleaned with deionized water. After this step, the slices were stained with acid fucsin (Sigma-Aldrich) for 5 minutes and then washed with deionized water. The samples were then immersed in a phosphotungstic acid/phosphomolybdic acid solution (Sigma-Aldrich) for 5 minutes and then stained with aniline blue for 5 minutes (Sigma-Aldrich). After this passage the slices were immersed in 1% acetic acid for 2 minutes, washed with deionized water and dehydrated with ethanol. Finally, the samples were clarified with xylene and mounted with the Eukitt mounting medium.

5.7 Adipocytes analysis

Adipocytes dimensions were evaluated on hematoxylin and eosin stained slices. At least 5 different fields were acquired with a 20X magnification under a Leica DM750 microscope equipped with a Leica ICC50W camera. The Adiposoft plugin of ImageJ was used to measure the adipocytes dimensions and the results were manually checked to assess the correct evaluation by the software.

5.8 RNA extraction and qRT-PCR

Mammary gland RNA extraction was performed using Trizol reagent (Roche Applied Science Mannheim) and homogenizing the specimen grinding the frozen tissue with MACS^{TM} Octo Dissociator (MACS Miltenyi Biotec). NanoDrop 3300 (Thermo Fisher Scientific Inc.) was used for total RNA spectrophotometric quantification and retro-transcription was achieved by using GoScript™ Reverse Transcription Mix, Random Primers (Promega), in accordance with provider's instructions. qRT-PCR with 2X SsoFast EvaGreen ready-to-use reaction cocktail (SsoFastTM EvaGreen® Supermix, Biorad) was conducted for target quantification. All the primers used for gene expression analysis were purchased from Sigma-Aldrich and are listed below. EvaGreen dye incorporation in the PCR products was monitored in real time using the CFX96 Touch Real-Time PCR Detection System (BioRad). Ct values were normalized over mGAPDH housekeeping gene.

Primers:

Murine ACC Fw:	5’ – CTGGCTGCATCCATTATGTCA – 3’
Murine ACC Rv:	5’ – TGGTAGACTGCCCGTGTGAA – 3’
Murine ELF5 Fw:	5’ – GTGGCATCAAGAGTCAAGACTGTC – 3’
Murine ELF5 Rv:	5’ – CTCAGCTTCTCGTACGTCATCCTG – 3’
Murine ER Fw:	5’ – CTGGACAGGAATCAAGGTAA – 3’
Murine ER Rv:	5’ – AGAAACGTGTACACTCCGG – 3’
Murine FASN Fw:	5’ – ATTGGTGGTGTGGACATGGTC – 3’
Murine FASN Rv:	5’ – CCCAGCCTTCCATCTCCTG – 3’
Murine GAPDH Fw:	5’ – TGACCACAGTCCATGCCATC – 3’
Murine GAPDH Rv:	5’ – GACGGACACATTGGGGGTAG – 3’
Murine LPL Fw:	5’ – CCAATGGAGGCACTTTCCA – 3’
Murine LPL Rv:	5’ – TGGTCCACGTCTCCGAGTC – 3’
Murine PgR Fw:	5’ – TATGGCGTGCTTACCTGTGG – 3’
Murine PgR Rv:	5’ – ACTTACGACCTCCAAGGAGGA – 3’
Murine PPARγ Fw:	5’ – TGTGGGGATAAAGCATCAGGC – 3’
Murine PPARγ Rv:	5’ – CCGGCAGTTAAGATCACACCTAT – 3’
Murine Prl-R Fw:	5’ – TGAGGACGAGCGGCTAATG – 3’
Murine Prl-R Rv:	5’ – GGTGTGTGGGTTTAACACCTTGA – 3’
Murine RANK-L Fw:	5’ – CAGCCGAGACTACGGCAAGT – 3’
Murine RANK-L Rv:	5’ – AGGATCCATCTGCGCTCGAAA – 3’
Murine SREBP-1C Fw:	5’ – GGAGCCATGGATTGCACATTTG – 3’
Murine SREBP-1C Rv:	5’ – CAAATAGGCCAGGGAAGTCAC – 3’
Murine TGF-β2 Fw:	5’ – TCCCCTCCGAAAATGCCATC – 3’
Murine TGF-β2 Rv:	5’ – ACTCTGCCTTCACCAGATTCG – 3’

5.9 Preparation of mammary gland lysates and Western Blot analysis

Total proteins were extracted from whole mammary gland by tissue disruption achieved through MACS^{TM} Octo Dissociator (MACS Miltenyi Biotec) and then quantified using Bradford protein assay ("Biorad Protein Assay" Bio Rad). Immunoblotting analysis were conducted first separating proteins in 4-20% SDS-PAGE (Criterion Precast Gel, Biorad) and then transferred to nitrocellulose membranes (GE Healthcare). 5% non-fat dried milk in TBS-0.1% Tween20 was used to block membranes and the incubation with primary antibody was performed ON at 4°C. Primary antibody used were: HER2 (Abcam, #ab134182), PgR (Termofisher, PA5-16440), ER (Termofisher, MA1-411), GAPDH (Cells Signaling, #5174) and Vinculin (Santa Cruz, sc7649, N19). Membranes were washed in TBS-0.1% Tween20 and incubated at RT for 1 hour with the appropriate horseradish peroxidase-conjugated secondary antibodies (GE Healthcare) for ECL detection (Clarity Western ECL Substrate, BioRad).

5.10 Statistical analysis

All the graphs and the statistical analyses were performed using Prism (version 7.00, GraphPad, Inc.). Data were compared using Student's t test or Mann-Whitney as appropriate and indicated below each figure. A minimum of three biologically independent specimens was used for statistical significance. Differences were considered significant at $P<0.05$.

6. REFERENCES

6. REFERENCES

1. Ali, S. & Coombes, R. C. Endocrine-responsive breast cancer and strategies for combating resistance. *Nat Rev Cancer* **2**, 101–112 (2002).
2. Andrechek, E. R., White, D. & Muller, W. J. Targeted disruption of ErbB2/Neu in the mammary epithelium results in impaired ductal outgrowth. *Oncogene* **24**, 932–937 (2005).
3. Antoniou, A. C. *et al.* A comprehensive model for familial breast cancer incorporating BRCA1, BRCA2 and other genes. *Br J Cancer* **86**, 76–83 (2002).
4. Asselin-Labat, M.-L. *et al.* Gata-3 is an essential regulator of mammary-gland morphogenesis and luminal-cell differentiation. *Nat Cell Biol* **9**, 201–209 (2007).
5. Bane, A. Ductal Carcinoma *In Situ* : What the Pathologist Needs to Know and Why. *International Journal of Breast Cancer* **2013**, 1–7 (2013).
6. Benson, J. R. *et al.* Early breast cancer. *The Lancet* **373**, 1463–1479 (2009).
7. Bergamaschi, A. *et al.* Extracellular matrix signature identifies breast cancer subgroups with different clinical outcome. *J. Pathol.* **214**, 357–367 (2008).
8. Bissell, M. J. & Hines, W. C. Why don't we get more cancer? A proposed role of the microenvironment in restraining cancer progression. *Nat Med* **17**, 320–329 (2011).
9. Blows, F. M. *et al.* Subtyping of Breast Cancer by Immunohistochemistry to Investigate a Relationship between Subtype and Short and Long Term Survival: A Collaborative Analysis of Data for 10,159 Cases from 12 Studies. *PLoS Med* **7**, e1000279 (2010).
10. Bonnans, C., Chou, J. & Werb, Z. Remodelling the extracellular matrix in development and disease. *Nat Rev Mol Cell Biol* **15**, 786–801 (2014).
11. Bouchard, L., Lamarre, L., Tremblay, P. J. & Jolicoeur, P. Stochastic appearance of mammary tumors in transgenic mice carrying the MMTV/c-neu oncogene. *Cell* **57**, 931–936 (1989).
12. Bressan, G. M. *et al.* Emilin, a component of elastic fibers preferentially located at the elastin-microfibrils interface. *Journal of Cell Biology* **121**, 201–212 (1993).

13. Bressan, G. M., Castellani, I., Colombatti, A. & Volpin, D. Isolation and characterization of a 115,000-dalton matrix-associated glycoprotein from chick aorta. *J Biol Chem* **258**, 13262–13267 (1983).

14. Brisken, C. *et al.* A paracrine role for the epithelial progesterone receptor in mammary gland development. *Proceedings of the National Academy of Sciences* **95**, 5076–5081 (1998).

15. Brisken, C. *et al.* Prolactin Controls Mammary Gland Development via Direct and Indirect Mechanisms. *Developmental Biology* **210**, 96–106 (1999).

16. Brown, K. A. Metabolic pathways in obesity-related breast cancer. *Nat Rev Endocrinol* **17**, 350–363 (2021).

17. Capuano, A. *et al.* Integrin binding site within the gC1q domain orchestrates EMILIN-1-induced lymphangiogenesis. *Matrix Biology* **81**, 34–49 (2019).

18. Capuano, A. *et al.* Abrogation of EMILIN1-β1 integrin interaction promotes experimental colitis and colon carcinogenesis. *Matrix Biology* **83**, 97–115 (2019).

19. Carey, L. A. *et al.* Race, Breast Cancer Subtypes, and Survival in the Carolina Breast Cancer Study. *JAMA* **295**, 2492 (2006).

20. Carioli, G. *et al.* European cancer mortality predictions for the year 2020 with a focus on prostate cancer. *Annals of Oncology* **31**, 650–658 (2020).

21. Carlson, R. W. The History and Mechanism of Action of Fulvestrant. *Clinical Breast Cancer* **6**, S5–S8 (2005).

22. Castagnoli, L. *et al.* Activated d16HER2 Homodimers and SRC Kinase Mediate Optimal Efficacy for Trastuzumab. *Cancer Res* **74**, 6248–6259 (2014).

23. Castiglioni, F. *et al.* Role of exon-16-deleted HER2 in breast carcinomas. *Endocr Relat Cancer* **13**, 221–232 (2006).

24. Chaudhuri, O. *et al.* Extracellular matrix stiffness and composition jointly regulate the induction of malignant phenotypes in mammary epithelium. *Nature Mater* **13**, 970–978 (2014).

25. Cheang, M. C. U. *et al.* Ki67 Index, HER2 Status, and Prognosis of Patients With Luminal B Breast Cancer. *JNCI: Journal of the National Cancer Institute* **101**, 736–750 (2009).

26. Choi, Y. S., Chakrabarti, R., Escamilla-Hernandez, R. & Sinha, S. Elf5 conditional knockout mice reveal its role as a master regulator in mammary alveolar development: Failure of Stat5 activation and functional differentiation in the absence of Elf5. *Developmental Biology* **329**, 227–241 (2009).

27. Clark, E. A. & Brugge, J. S. Integrins and Signal Transduction Pathways: the Road Taken. *Science* **268**, 233–239 (1995).

28. Colombatti, A. *et al.* The EMILIN protein family. *Matrix Biology* **19**, 289–301 (2000).

29. Colombatti, A. *et al.* The EMILIN/Multimerin Family. *Front. Immun.* **2**, (2012).

30. Danussi, C. *et al.* EMILIN1–α4/α9 integrin interaction inhibits dermal fibroblast and keratinocyte proliferation. *Journal of Cell Biology* **195**, 131–145 (2011).

31. Danussi, C. *et al.* An EMILIN1-Negative Microenvironment Promotes Tumor Cell Proliferation and Lymph Node Invasion. *Cancer Prev Res* **5**, 1131–1143 (2012).

32. Danussi, C. *et al. Emilin1* Deficiency Causes Structural and Functional Defects of Lymphatic Vasculature. *Mol Cell Biol* **28**, 4026–4039 (2008).

33. Davis, K. R. *et al.* XBP1 Regulates the Biosynthetic Capacity of the Mammary Gland During Lactation by Controlling Epithelial Expansion and Endoplasmic Reticulum Formation. *Endocrinology* **157**, 417–428 (2016).

34. Dawood, S. Triple-Negative Breast Cancer: Epidemiology and Management Options. *Drugs* **70**, 2247–2258 (2010).

35. Desmedt, C. *et al.* Biological Processes Associated with Breast Cancer Clinical Outcome Depend on the Molecular Subtypes. *Clin Cancer Res* **14**, 5158–5165 (2008).

36. Doliana, R., Bot, S., Bonaldo, P. & Colombatti, A. EMI, a novel cysteine-rich domain of EMILINs and other extracellular proteins, interacts with the gC1q domains and participates in multimerization. *FEBS Letters* **484**, 164–168 (2000).

37. Fata, J. E. *et al.* The Osteoclast Differentiation Factor Osteoprotegerin-Ligand Is Essential for Mammary Gland Development. *Cell* **103**, 41–50 (2000).

38. Feng, Y., Manka, D., Wagner, K.-U. & Khan, S. A. Estrogen receptor- expression in the mammary epithelium is required for ductal and alveolar morphogenesis in mice. *Proceedings of the National Academy of Sciences* **104**, 14718–14723 (2007).

39. Ferraro, G. B. *et al.* Fatty acid synthesis is required for breast cancer brain metastasis. *Nat Cancer* **2**, 414–428 (2021).

40. Finkle, D. *et al.* HER2-Targeted Therapy Reduces Incidence and Progression of Midlife Mammary Tumors in Female Murine Mammary Tumor Virus huHER2-Transgenic Mice. *Clin Cancer Res* **10**, 2499–2511 (2004).

41. Gallego, M. I. *et al.* Prolactin, Growth Hormone, and Epidermal Growth Factor Activate Stat5 in Different Compartments of Mammary Tissue and Exert Different and Overlapping Developmental Effects. *Developmental Biology* **229**, 163–175 (2001).

42. Gilcrease, M. Z. Integrin signaling in epithelial cells. *Cancer Letters* **247**, 1–25 (2007).

43. Gkretsi, V. & Stylianopoulos, T. Cell Adhesion and Matrix Stiffness: Coordinating Cancer Cell Invasion and Metastasis. *Front. Oncol.* **8**, 145 (2018).

44. Guy, C. T., Cardiff, R. D. & Muller, W. J. Activated neu Induces Rapid Tumor Progression. *Journal of Biological Chemistry* **271**, 7673–7678 (1996).

45. Harris, J. *et al.* Socs2 and Elf5 Mediate Prolactin-Induced Mammary Gland Development. *Molecular Endocrinology* **20**, 1177–1187 (2006).

46. Hart, V., Gautrey, H., Kirby, J. & Tyson-Capper, A. HER2 splice variants in breast cancer: investigating their impact on diagnosis and treatment outcomes. *Oncotarget* **11**, 4338–4357 (2020).

47. Henke, E., Nandigama, R. & Ergün, S. Extracellular Matrix in the Tumor Microenvironment and Its Impact on Cancer Therapy. *Front. Mol. Biosci.* **6**, 160 (2020).

48. Hennighausen, L. & Robinson, G. W. Information networks in the mammary gland. *Nat Rev*

Mol Cell Biol **6**, 715–725 (2005).

49. Hergueta-Redondo, M., Palacios, J., Cano, A. & Moreno-Bueno, G. "New" molecular taxonomy in breast cancer. *Clin Transl Oncol* **10**, 777–785 (2008).
50. Higgins, M. J. & Baselga, J. Targeted therapies for breast cancer. *J. Clin. Invest.* **121**, 3797–3803 (2011).
51. Holbro, T. & Hynes, N. E. ErbB Receptors: Directing Key Signaling Networks Throughout Life. *Annu. Rev. Pharmacol. Toxicol.* **44**, 195–217 (2004).
52. Huang, J. *et al.* Extracellular matrix and its therapeutic potential for cancer treatment. *Sig Transduct Target Ther* **6**, 153 (2021).
53. Hynes, N. E. & Watson, C. J. Mammary Gland Growth Factors: Roles in Normal Development and in Cancer. *Cold Spring Harbor Perspectives in Biology* **2**, a003186–a003186 (2010).
54. Hynes, N. E. & MacDonald, G. ErbB receptors and signaling pathways in cancer. *Current Opinion in Cell Biology* **21**, 177–184 (2009).
55. Iacomino, M. *et al.* Distal motor neuropathy associated with novel EMILIN1 mutation. *Neurobiology of Disease* **137**, 104757 (2020).
56. Inman, J. L., Robertson, C., Mott, J. D. & Bissell, M. J. Mammary gland development: cell fate specification, stem cells and the microenvironment. *Development* **142**, 1028–1042 (2015).
57. Jackson-Fisher, A. J. *et al.* ErbB2 is required for ductal morphogenesis of the mammary gland. *Proceedings of the National Academy of Sciences* **101**, 17138–17143 (2004).
58. Jacquemier, J. *et al.* Association of GATA3, P53, Ki67 status and vascular peritumoral invasion are strongly prognostic in luminal breast cancer. *Breast Cancer Res* **11**, R23 (2009).
59. Jatoi, I., Hilsenbeck, S. G., Clark, G. M. & Osborne, C. K. Significance of Axillary Lymph Node Metastasis in Primary Breast Cancer. *JCO* **17**, 2334–2334 (1999).
60. Jin, H. A homing mechanism for bone marrow-derived progenitor cell recruitment to the neovasculature. *Journal of Clinical Investigation* **116**, 652–662 (2006).

61. Jin, H., Su, J., Garmy-Susini, B., Kleeman, J. & Varner, J. Integrin $\alpha_4\beta_1$ Promotes Monocyte Trafficking and Angiogenesis in Tumors. *Cancer Res* **66**, 2146–2152 (2006).

62. Kalli, M. & Stylianopoulos, T. Defining the Role of Solid Stress and Matrix Stiffness in Cancer Cell Proliferation and Metastasis. *Front. Oncol.* **8**, 55 (2018).

63. Kalluri, R. & Neilson, E. G. Epithelial-mesenchymal transition and its implications for fibrosis. *J. Clin. Invest.* **112**, 1776–1784 (2003).

64. Kalluri, R. & Weinberg, R. A. The basics of epithelial-mesenchymal transition. *J. Clin. Invest.* **119**, 1420–1428 (2009).

65. Klauber-DeMore, N. *et al.* Size of Residual Lymph Node Metastasis After Neoadjuvant Chemotherapy in Locally Advanced Breast Cancer Patients Is Prognostic. *Ann Surg Oncol* **13**, 685–691 (2006).

66. Koletsa, T. *et al.* A Splice Variant of HER2 Corresponding to Herstatin Is Expressed in the Noncancerous Breast and in Breast Carcinomas. *Neoplasia* **10**, 687–696 (2008).

67. Kouros-Mehr, H., Slorach, E. M., Sternlicht, M. D. & Werb, Z. GATA-3 Maintains the Differentiation of the Luminal Cell Fate in the Mammary Gland. *Cell* **127**, 1041–1055 (2006).

68. Kumagai, S., Koyama, S. & Nishikawa, H. Antitumour immunity regulated by aberrant ERBB family signalling. *Nat Rev Cancer* **21**, 181–197 (2021).

69. Lamy, P.-J. *et al.* Quantification and clinical relevance of gene amplification at chromosome 17q12-q21 in human epidermal growth factor receptor 2-amplified breast cancers. *Breast Cancer Res* **13**, R15 (2011).

70. Lauby-Secretan, B. *et al.* Body Fatness and Cancer — Viewpoint of the IARC Working Group. *N Engl J Med* **375**, 794–798 (2016).

71. Levental, K. R. *et al.* Matrix Crosslinking Forces Tumor Progression by Enhancing Integrin Signaling. *Cell* **139**, 891–906 (2009).

72. Li, C. I., Uribe, D. J. & Daling, J. R. Clinical characteristics of different histologic types of breast cancer. *Br J Cancer* **93**, 1046–1052 (2005).

73. Lydon, J. P. *et al.* Mice lacking progesterone receptor exhibit pleiotropic reproductive abnormalities. *Genes Dev.* **9**, 2266–2278 (1995).

74. Malhotra, G. K., Zhao, X., Band, H. & Band, V. Histological, molecular and functional subtypes of breast cancers. *Cancer Biology & Therapy* **10**, 955–960 (2010).

75. Malvezzi, M. *et al.* European cancer mortality predictions for the year 2019 with focus on breast cancer. *Annals of Oncology* **30**, 781–787 (2019).

76. Mani, S. A. *et al.* The Epithelial-Mesenchymal Transition Generates Cells with Properties of Stem Cells. *Cell* **133**, 704–715 (2008).

77. Marchini, C. *et al.* The Human Splice Variant Δ16HER2 Induces Rapid Tumor Onset in a Reporter Transgenic Mouse. *PLoS ONE* **6**, e18727 (2011).

78. Marchini, C. *et al.* HER2-Driven Carcinogenesis: New Mouse Models for Novel Immunotherapies. in *Oncogene and Cancer - From Bench to Clinic* (ed. Siregar, Y.) (InTech, 2013). doi:10.5772/53880.

79. Massat, N. J. *et al.* Explaining the Better Prognosis of Screening-Exposed Breast Cancers: Influence of Tumor Characteristics and Treatment. *Cancer Epidemiol Biomarkers Prev* **25**, 479–487 (2016).

80. McPherson, K. ABC of breast diseases: Breast cancer---epidemiology, risk factors, and genetics. *BMJ* **321**, 624–628 (2000).

81. Melchor, L. & Benítez, J. The complex genetic landscape of familial breast cancer. *Hum Genet* **132**, 845–863 (2013).

82. Mishra, R., Hanker, A. B. & Garrett, J. T. Genomic alterations of ERBB receptors in cancer: clinical implications. *Oncotarget* **8**, 114371–114392 (2017).

83. Mitra, D. *et al.* An oncogenic isoform of HER2 associated with locally disseminated breast cancer and trastuzumab resistance. *Mol Cancer Ther* **8**, 2152–2162 (2009).

84. Moasser, M. M. The oncogene HER2: its signaling and transforming functions and its role in human cancer pathogenesis. *Oncogene* **26**, 6469–6487 (2007).

85. Modica, T. M. E. *et al.* The extracellular matrix protein EMILIN1 silences the RAS-ERK pathway via α4β1 integrin and decreases tumor cell growth. *Oncotarget* **8**, 27034–27046 (2017).

86. Moody, S. E. *et al.* Conditional activation of Neu in the mammary epithelium of transgenic mice results in reversible pulmonary metastasis. *Cancer Cell* **2**, 451–461 (2002).

87. Muller, W. J., Sinn, E., Pattengale, P. K., Wallace, R. & Leder, P. Single-step induction of mammary adenocarcinoma in transgenic mice bearing the activated c-neu oncogene. *Cell* **54**, 105–115 (1988).

88. Nelson, C. M., VanDuijn, M. M., Inman, J. L., Fletcher, D. A. & Bissell, M. J. Tissue Geometry Determines Sites of Mammary Branching Morphogenesis in Organotypic Cultures. *Science* **314**, 298–300 (2006).

89. Olayioye, M. A. NEW EMBO MEMBERS' REVIEW: The ErbB signaling network: receptor heterodimerization in development and cancer. *The EMBO Journal* **19**, 3159–3167 (2000).

90. Ormandy, C. J., Binart, N. & Kelly, P. A. [No title found]. *Journal of Mammary Gland Biology and Neoplasia* **2**, 355–364 (1997).

91. Parise, C. A., Bauer, K. R., Brown, M. M. & Caggiano, V. Breast Cancer Subtypes as Defined by the Estrogen Receptor (ER), Progesterone Receptor (PR), and the Human Epidermal Growth Factor Receptor 2 (HER2) among Women with Invasive Breast Cancer in California, 1999-2004. *The Breast Journal* **15**, 593–602 (2009).

92. Parmar, H. & Cunha, G. R. Epithelial–stromal interactions in the mouse and human mammary gland in vivo. *Endocr Relat Cancer* **11**, 437–458 (2004).

93. Perou, C. M. & Borresen-Dale, A.-L. Systems Biology and Genomics of Breast Cancer. *Cold Spring Harbor Perspectives in Biology* **3**, a003293–a003293 (2011).

94. Perou, C. M., Parker, J. S., Prat, A., Ellis, M. J. & Bernard, P. S. Clinical implementation of the intrinsic subtypes of breast cancer. *The Lancet Oncology* **11**, 718–719 (2010).

95. Perou, C. M. *et al.* Molecular portraits of human breast tumours. *Nature* **406**, 747–752 (2000).

96. Piechocki, M. P., Ho, Y.-S., Pilon, S. & Wei, W.-Z. Human ErbB-2 (Her-2) Transgenic Mice: A Model System for Testing Her-2 Based Vaccines. *J Immunol* **171**, 5787–5794 (2003).

97. Pivetta, E. *et al.* Neutrophil elastase-dependent cleavage compromises the tumor suppressor role of EMILIN1. *Matrix Biology* **34**, 22–32 (2014).

98. Prat, A. *et al.* Phenotypic and molecular characterization of the claudin-low intrinsic subtype of breast cancer. *Breast Cancer Res* **12**, R68 (2010).

99. Qi, Y. *et al.* TSPAN9 and EMILIN1 synergistically inhibit the migration and invasion of gastric cancer cells by increasing TSPAN9 expression. *BMC Cancer* **19**, 630 (2019).

100. Rabajdova, M. *et al.* The crucial role of emilin 1 gene expression during progression of tumor growth. *J Cancer Res Clin Oncol* **142**, 2397–2402 (2016).

101. Rakha, E. A., Reis-Filho, J. S. & Ellis, I. O. Basal-Like Breast Cancer: A Critical Review. *JCO* **26**, 2568–2581 (2008).

102. Richards, M., Westcombe, A., Love, S., Littlejohns, P. & Ramirez, A. Influence of delay on survival in patients with breast cancer: a systematic review. *The Lancet* **353**, 1119–1126 (1999).

103. Röhrig, F. & Schulze, A. The multifaceted roles of fatty acid synthesis in cancer. *Nat Rev Cancer* **16**, 732–749 (2016).

104. Sasso, M., Bianchi, F., Ciravolo, V., Tagliabue, E. & Campiglio, M. HER2 splice variants and their relevance in breast cancer. *J Nucleic Acids Invest* **2**, 9 (2011).

105. Schiavinato, A. *et al.* Fibulin-4 deposition requires EMILIN-1 in the extracellular matrix of osteoblasts. *Sci Rep* **7**, 5526 (2017).

106. Schiavinato, A. *et al.* Targeting of EMILIN-1 and EMILIN-2 to Fibrillin Microfibrils Facilitates their Incorporation into the Extracellular Matrix. *Journal of Investigative Dermatology* **136**, 1150–1160 (2016).

107. Slamon, D. J. *et al.* Use of Chemotherapy plus a Monoclonal Antibody against HER2 for Metastatic Breast Cancer That Overexpresses HER2. *N Engl J Med* **344**, 783–792 (2001).

108. Sorlie, T. *et al.* Gene expression patterns of breast carcinomas distinguish tumor subclasses with clinical implications. *Proceedings of the National Academy of Sciences* **98**, 10869–10874 (2001).

109. Sørlie, T. *et al.* Repeated observation of breast tumor subtypes in independent gene expression data sets. *PNAS* **100**, 8418–8423 (2003).

110. Sotiriou, C. & Pusztai, L. Gene-Expression Signatures in Breast Cancer. *N Engl J Med* **360**, 790–800 (2009).

111. Spessotto, P. *et al.* β1 Integrin-dependent Cell Adhesion to EMILIN-1 Is Mediated by the gC1q Domain. *Journal of Biological Chemistry* **278**, 6160–6167 (2003).

112. Spitale, A., Mazzola, P., Soldini, D., Mazzucchelli, L. & Bordoni, A. Breast cancer classification according to immunohistochemical markers: clinicopathologic features and short-term survival analysis in a population-based study from the South of Switzerland. *Annals of Oncology* **20**, 628–635 (2009).

113. Streuli, C. H. Integrins and cell-fate determination. *Journal of Cell Science* **122**, 171–177 (2009).

114. Suzuki, R., Kohno, H., Sugie, S., Nakagama, H. & Tanaka, T. Strain differences in the susceptibility to azoxymethane and dextran sodium sulfate-induced colon carcinogenesis in mice. *Carcinogenesis* **27**, 162–169 (2005).

115. Tanaka, T. *et al.* A novel inflammation-related mouse colon carcinogenesis model induced by azoxymethane and dextran sodium sulfate. *Cancer Science* **94**, 965–973 (2003).

116. Tang, V. W. Collagen, stiffness, and adhesion: the evolutionary basis of vertebrate mechanobiology. *MBoC* **31**, 1823–1834 (2020).

117. Tsuda, H. Prognostic and predictive value of c-erbB-2 (HER-2/neu) gene amplification in human Breast Cancer. *Breast Cancer* **8**, 38–44 (2001).

118. Turpin, J. *et al.* The ErbB2ΔEx16 splice variant is a major oncogenic driver in breast cancer that promotes a pro-metastatic tumor microenvironment. *Oncogene* **35**, 6053–6064 (2016).

119. Venkitaraman, A. R. Cancer Susceptibility and the Functions of BRCA1 and BRCA2. *Cell* **108**, 171–182 (2002).

120. Visvader, J. E. Keeping abreast of the mammary epithelial hierarchy and breast tumorigenesis. *Genes Dev.* **23**, 2563–2577 (2009).

121. Vogel, C. L. *et al.* Efficacy and Safety of Trastuzumab as a Single Agent in First-Line Treatment of *HER2* -Overexpressing Metastatic Breast Cancer. *JCO* **20**, 719–726 (2002).

122. Walker, J. L. & Assoian, R. K. Integrin-dependent signal transduction regulating cyclin D1 expression and G1 phase cell cycle progression. *Cancer Metastasis Rev* **24**, 383–393 (2005).

123. Wang, S. H. *et al.* Characterization of a Novel Transgenic Mouse Tumor Model for Targeting HER2+ Cancer Stem Cells. *Int. J. Biol. Sci.* **10**, 25–32 (2014).

124. Wang, Y. *et al.* Cancer-associated fibroblast-derived SDF-1 induces epithelial-mesenchymal transition of lung adenocarcinoma via CXCR4/β-catenin/PPARδ signalling. *Cell Death Dis* **12**, 214 (2021).

125. Weigelt, B., Baehner, F. L. & Reis-Filho, J. S. The contribution of gene expression profiling to breast cancer classification, prognostication and prediction: a retrospective of the last decade: A commentary on microarrays in breast cancer research. *J. Pathol.* **220**, 263–280 (2010).

126. Wells, R. G. The role of matrix stiffness in regulating cell behavior. *Hepatology* **47**, 1394–1400 (2008).

127. Xu, J., Lamouille, S. & Derynck, R. TGF-β-induced epithelial to mesenchymal transition. *Cell Res* **19**, 156–172 (2009).

128. Yu, Y. *et al.* Cancer-associated fibroblasts induce epithelial–mesenchymal transition of breast cancer cells through paracrine TGF-β signalling. *Br J Cancer* **110**, 724–732 (2014).

129. Zacchigna, L. *et al.* Emilin1 Links TGF-β Maturation to Blood Pressure Homeostasis. *Cell* **124**, 929–942 (2006).

130. Zanetti, M. *et al.* EMILIN-1 Deficiency Induces Elastogenesis and Vascular Cell Defects. *Mol Cell Biol* **24**, 638–650 (2004).

131. Zhang, S. D., Kassis, J., Olde, B., Mellerick, D. M. & Odenwald, W. F. Pollux, a novel Drosophila adhesion molecule, belongs to a family of proteins expressed in plants, yeast, nematodes, and man. *Genes Dev.* **10**, 1108–1119 (1996).

132. Zhang, S. *et al.* Combating trastuzumab resistance by targeting SRC, a common node downstream of multiple resistance pathways. *Nat Med* **17**, 461–469 (2011).

133. Zhou, J. *et al.* Elf5 is essential for early embryogenesis and mammary gland development during pregnancy and lactation. *EMBO J* **24**, 635–644 (2005).

7. PUBLICATIONS

7. PUBLICATIONS

Andreuzzi, E., Capuano, A., Poletto, E., Pivetta, E., Fejza, A., **Favero, A.**, Doliana, R., Cannizzaro, R., Spessotto, P., Mongiat, M., 2020a. Role of Extracellular Matrix in Gastrointestinal Cancer-Associated Angiogenesis. IJMS 21, 3686. https://doi.org/10.3390/ijms21103686

Andreuzzi, E., Fejza, A., Capuano, A., Poletto, E., Pivetta, E., Doliana, R., Pellicani, R., **Favero, A.**, Maiero, S., Fornasarig, M., Cannizzaro, R., Iozzo, R.V., Spessotto, P., Mongiat, M., 2020b. Deregulated expression of Elastin Microfibril Interfacer 2 (EMILIN2) in gastric cancer affects tumor growth and angiogenesis. Matrix Biology Plus 6–7, 100029. https://doi.org/10.1016/j.mbplus.2020.100029

Capuano, A., Andreuzzi, E., Pivetta, E., Doliana, R., **Favero, A.**, Canzonieri, V., Maiero, S., Fornasarig, M., Magris, R., Cannizzaro, R., Mongiat, M., Spessotto, P., 2019a. The Probe Based Confocal Laser Endomicroscopy (pCLE) in Locally Advanced Gastric Cancer: A Powerful Technique for Real–Time Analysis of Vasculature. Front. Oncol. 9, 513. https://doi.org/10.3389/fonc.2019.00513

Capuano, A., Pivetta, E., Sartori, G., Bosisio, G., **Favero, A.**, Cover, E., Andreuzzi, E., Colombatti, A., Cannizzaro, R., Scanziani, E., Minoli, L., Bucciotti, F., Amor Lopez, A.I., Gaspardo, K., Doliana, R., Mongiat, M., Spessotto, P., 2019b. Abrogation of EMILIN1-β1 integrin interaction promotes experimental colitis and colon carcinogenesis. Matrix Biology 83, 97–115. https://doi.org/10.1016/j.matbio.2019.08.006

Casagrande, N., Borghese, C., **Favero, A.**, Vicenzetto, C., Aldinucci, D., 2021. Trabectedin overcomes doxorubicin-resistance, counteracts tumor-immunosuppressive reprogramming of monocytes and decreases xenograft growth in Hodgkin lymphoma. Cancer Letters 500, 182–193. https://doi.org/10.1016/j.canlet.2020.12.015

Citron, F., Segatto, I., Musco, L., Pellarin, I., Rampioni Vinciguerra, G.L., Franchin, G., Fanetti, G., Miccichè, F., Giacomarra, V., Lupato, V., **Favero, A.**, Concina, I., Srinivasan, S., Avanzo, M., Castiglioni, I., Barzan, L., Sulfaro, S., Petrone, G., Viale, A., Draetta, G.F., Vecchione, A., Belletti, B., Baldassarre, G., 2021. miR-9 modulates and predicts the response to radiotherapy and EGFR inhibition in HNSCC. EMBO Mol Med 13. https://doi.org/10.15252/emmm.202012872

Favero, A., Segatto, I., Perin, T., Belletti, B., 2021. The many facets of MIR -223 in cancer: Oncosuppressor, oncogenic driver, therapeutic target, and biomarker of response. WIREs RNA 12. https://doi.org/10.1002/wrna.1659

Rampioni Vinciguerra, G.L., Dall'Acqua, A., Segatto, I., Mattevi, M.C., Russo, F., **Favero, A.**, Cirombella, R., Mungo, G., Viotto, D., Karimbayli, J., Pesce, M., Vecchione, A., Belletti, B., Baldassarre, G., 2021. p27kip1 expression and phosphorylation dictate Palbociclib sensitivity in KRAS-mutated colorectal cancer. Cell Death Dis 12, 951. https://doi.org/10.1038/s41419-021-04241-2

8. Acknowledgements

Throughout this 3-years PhD I have received a great deal of support and assistance. I would first like to thank my supervisors, Dr. Paola Spessotto and Dr. Barbara Belletti for their valuable guidance. You helped me to choose the right direction for my project and to write the final thesis. I would like to acknowledge my colleagues from the Molecular Oncology unit at CRO Aviano for their wonderful collaboration. You supported me greatly and were always willing to help me.